PNAS

Main Manuscript for

Protease-mediated degradation of the master transcription factor controls quorum sensing-state transitions in *Vibrio*

Tanmaya A. Rasal[1], Caleb P. Mallery[2], Biqing Liang[2], Matthew W. Brockley[3], Chelsea A. Simpson,[1] Abigail D. Padgett[1], Finley J. Andrew[4], Laura C. Brown[5], Jon E. Paczkowski[2,3*], Julia C. van Kessel[1*]

1. Department of Biology, Indiana University, Bloomington, IN.
2. Department of Biomedical Sciences, University of Albany, Albany, NY.
3. Division of Genetics, Wadsworth Center, New York State Department of Health, Albany, NY.
4. Ryan White Center for Pediatric Infectious Diseases and Global Health, Herman B. Wells Center for Pediatric Research, Department of Pediatrics, Indiana University School of Medicine, Indianapolis, IN
5. Department of Chemistry, Indiana University, Bloomington, IN

* Corresponding authors:
Dr. Julia van Kessel
Biology Building 425K, Department of Biology, Indiana University
1001 E 3rd Street, Bloomington, IN 47405
Email: jcvk@iu.edu
Telephone: 812-856-2235

Dr. Jon Paczkowski
David Axelrod Institute LSIB 5221, Division of Genetics, Wadsworth Center, NYSDOH
120 New Scotland Avenue, Albany, NY 12208
Email: jon.paczkowski@health.ny.gov
Telephone: 518-474-5484

Author contributions: JVK, JEP, LCB, and TAR designed the research, TAR, CPM, MWB, BL, CAS, ADP, FJA, JEP, and JVK performed experiments, JVK, JEP, LCB, CPM, and TAR analyzed data, and JVK, JEP, LCB, TAR, and CPM wrote the manuscript.

Competing Interests Statement: JVK and LCB disclose their relationship with the company Quornix, LLC as board members and co-founders. Both JVK and LCB have a patent pending for

35 thiophenesulfonamide compounds and their methods of use (application number 63/064,963). All other
36 authors declare that they have no competing interests.
37
38 **Classification:** Biological Sciences, Microbiology
39
40 **Keywords:** Quorum sensing inhibitors, *Vibrio vulnificus*, SmcR, thiophenesulfonamides, protease
41
42 **This PDF file includes:**
43 Main Text
44 Figures 1 to 7

Abstract

In *Vibrio* species, quorum sensing signaling culminates in the production of the master transcription factor SmcR that regulates group behavior genes in a density-dependent manner. Previously, we identified a small molecule thiophenesulfonamide inhibitor called PTSP that targets the SmcR family of proteins and blocks activity *in vivo*. Here, we used structure-function analyses to identify eight PTSP-interacting residues in the ligand binding pocket that are required for PTSP inhibition of *Vibrio vulnificus* SmcR. Binding of PTSP to SmcR drives allosteric unfolding of the N-terminal DNA-binding domain and, in this state, SmcR is degraded by the ClpAP protease. SmcR degradation controls the timing of the phenotypic switch between high and low cell density, and strains expressing degradation-resistant *smcR* alleles are impervious to changes in cell density state. These studies implicate ligand binding as a mediator of SmcR protein stability and function, which dictates the timing of quorum sensing gene expression in three *Vibrio* pathogens.

Significance Statement

SmcR family proteins were discovered in the 1990s as central regulators of quorum sensing gene expression and later discovered to be conserved in all studied *Vibrio* species. SmcR homologs regulate a wide range of genes involved in pathogenesis, including but not limited to genes involved in biofilm production and toxin secretion. As archetypal members of the broad class of TetR-type transcription factors, each SmcR type protein has a predicted ligand binding pocket. However, no ligand has been identified for these proteins that control their function as regulators. Here, we used SmcR-specific chemical inhibitors to determine that ligand binding drives proteolytic degradation *in vivo*, the first demonstration of SmcR function connected to ligand binding for this historical protein family.

Introduction

Among the >100 species of *Vibrionaceae* that inhabit marine environments, *Vibrio vulnificus* is one of the most potent human pathogens with a mortality rate of >50% in primary septicemia infections (1–3). Historically, infections were endemic to equatorial regions but due to a global rise in temperatures, there has been an alarming increase and spread of vibriosis to regions beyond their typical equatorial habitats (2–4). This has consequently caused worldwide harm to aquaculture industries, natural marine ecosystems, and human health (7–10). Additionally, *Vibrio* species have been shown to evolve by gaining fitness traits through horizontal gene transfer (HGT), including genes encoding multidrug resistance (9, 10). The emergence of multidrug resistant *Vibrio* strains has prompted a need to develop alternative strategies to treat vibriosis.

In *Vibrio* species, one major regulatory system that controls expression of virulence genes is quorum sensing (QS), a cell-to-cell signaling system that allows bacteria to control group behaviors in

80 response to alterations in population density (11–13). The model presented in **Figure S1** depicts the QS
81 signaling system defined in *Vibrio campbellii*. At low cell density (LCD), autoinducer concentrations are
82 low, and multiple unbound receptors act as kinases to phosphorylate LuxU, the phosphotransfer protein.
83 LuxU phosphorylates the response regulator LuxO, and phosphorylated LuxO, together with σ-54,
84 activates expression of the five Qrr small RNAs (16). The Qrrs repress the master QS transcription factor,
85 a family of proteins only found in *Vibrios* and collectively called the LuxR/HapR family (17). The Qrrs also
86 activate translation of the LCD regulator AphA, leading to expression of genes for individual behaviors
87 (16–18). At high cell density (HCD), binding of autoinducers and/or nitric oxide (19, 20) to the receptors
88 changes their activities to those of phosphatases, resulting in dephosphorylated LuxO and loss of Qrr
89 expression. Thus, production of LuxR/HapR is highest at HCD, and this master transcription factor
90 regulates the expression of genes encoding for proteins with various functions (19, 20, 23). The master
91 QS transcriptional regulators in each *Vibrio* species, *e.g.*, *V. campbellii* LuxR, *V. cholerae* HapR, *V.*
92 *parahaemolyticus* OpaR, and *V. vulnificus* SmcR, are highly conserved in pathogenic *Vibrios* and are
93 important regulators of virulence gene expression (17, 24). These proteins are not structurally or
94 functionally the same as the LuxR-type proteins found associated with LuxI acyl-homoserine lactone
95 synthases in other Gram-negative bacterial QS systems (12, 23, 24). Rather, the master QS transcription
96 factors that we discuss here called the LuxR/HapR family are part of the broad TetR family of proteins.
97 TetR proteins are characterized by homodimeric complexes with an N-terminal helix-turn-helix DNA
98 binding domain (DBD) and a C-terminal dimerization domain with a putative ligand-binding pocket (LBP),
99 which typically mediates the conformation of the DBD. Thus, TetR DNA-binding activity is classically
100 controlled in a ligand-dependent manner (27). Crystal structures of SmcR and HapR revealed a putative
101 LBP near the dimerization domain that is characterized by hydrophobic residues and is hypothesized to
102 contain an unidentified native ligand (23, 24). However, no ligand has been identified to date. Thus,
103 functional studies of the LuxR/HapR family of proteins and their ligand binding partners have been limited.
104 Because LuxR/HapR proteins are the central regulators of QS signaling genes, they have been a
105 focus of research since their discovery (28). Indeed, their importance in *Vibrio* virulence gene regulation is
106 well-documented; deletion of *smcR* or inhibition of SmcR in *V. vulnificus* decreases pathogenesis in both
107 mouse and shrimp models (29, 30). Recent studies have shown that QS inhibitors are feasible
108 alternatives to traditional antibiotics with demonstrated efficacy in infection models (31, 32). Because
109 these inhibitors do not affect bacterial viability, they are hypothesized to generate less selective pressure
110 for evolving resistance (33, 34). LuxR/HapR-specific inhibitors have been identified via *in vitro* and *in*
111 *silico* screening efforts and include molecules with functional groups such as aromatic sulfonamides,
112 enones, sulfones, furanones, brominated thiophenones, and cinnamaldehydes (35–41). Each of these
113 inhibits QS phenotypes to some degree in *V. campbellii* and/or other *Vibrio* species. However, most of
114 these either did not result in large changes in QS or required high concentrations to be effective. Kim *et.*
115 *al.* identified a selective *Vibrio* QS inhibitor named Qstatin [1-(5-bromothiophene-2-sulfonyl)-1H-pyrazole],
116 which inhibits *V. vulnificus* SmcR (29). Based on biochemical assays, they hypothesized that Qstatin

117 binds to the putative LBP in SmcR, changing the entropic and enthalpic components of the system and
118 altering SmcR regulatory activity *in vivo*. Their data showed that Qstatin resulted in SmcR dysfunction,
119 eliminating the expression of the SmcR regulon required for virulence, biofilm dynamics, and
120 motility/chemotaxis. Qstatin markedly attenuated different representative QS-regulated phenotypes in the
121 test *Vibrio* species, including virulence against the brine shrimp (*Artemia franciscana*) (29). However, the
122 mechanism of action of Qstatin was not clear; addition of Qstatin did not alter DNA binding more than 2-
123 fold *in vitro* (29), and that result was not observed in DNA binding assays performed by our group (42).
124 Subsequently, our group synthesized a panel of thiophenesulfonamide inhibitors and screened
125 them for their inhibitory activity against different LuxR/HapR proteins. We identified several compounds
126 that displayed equal or better efficacy compared to Qstatin against LuxR/HapR homologs in various
127 *Vibrio* species with no impact on bacterial viability (43). From that panel, PTSP (3-**p**henyl-1-(**t**hiophen-2-
128 yl**s**ulfonyl)-1*H*-**p**yrazole) was the most effective inhibitor (**Fig. 1A**). It is structurally different from Qstatin
129 such that it has an additional phenyl group on the pyrazole ring of the molecule and no bromine on the
130 thiophene ring. It inhibits LuxR/HapR homologs in different *Vibrio* species at nanomolar to micromolar
131 concentrations with distinct efficacies based on their respective putative LBP (41). PTSP shows the
132 strongest inhibition of *V. vulnificus* SmcR but does not inhibit *V. cholerae* HapR. Based on these results,
133 the Raychaudhuri lab sought to determine the molecular basis of HapR insensitivity to Qstatin and its
134 derivatives (44). They constructed a variant HapR by replacing four native LBP residues with SmcR
135 residues, two of which our group had shown to be necessary for SmcR sensitivity to PTSP. They made
136 single, double, triple, and quadruple substitution mutants at residues Y76F, L97I, I141V and F171C (43,
137 44). Their assays showed that only the quadruple mutant was susceptible to Qstatin and its phenyl
138 derivative inhibitor called IMT-VC-212 (44).
139 Here, we used a genetic screen and biophysical techniques to determine PTSP interactions with
140 SmcR. Our results show that multiple residues in the LBP of SmcR are critical for PTSP binding *in vivo*.
141 Substitutions at residues in the LBP abrogate PTSP inhibition and restore wild-type activity to SmcR *in*
142 *vivo*. PTSP binding to SmcR increases protein degradation by the ClpAP protease *in vivo.* Clp proteases
143 belong to the highly conserved ATP-dependent proteases- these are composed of a proteolytic core
144 (ClpP) and one or more unfoldases (ClpA, ClpC, ClpX, etc.). They play a crucial role in protein quality
145 control and removal of damaged or misfolded proteins (45, 46). We also observed that SmcR variants
146 that are resistant to PTSP were not susceptible to this degradation. Thus, the mechanism of
147 thiophenesulfonamide inhibition of SmcR is driven by proteolysis *in vivo*, indicating that the stability of
148 SmcR, and possibly its conformation, is connected to interactions with the compound in its LBP. This
149 mechanism was observed in multiple *Vibrio* species. Moreover, ClpAP-mediated turnover of SmcR
150 impacts the transitions between LCD and HCD signaling states, broadly implicating the importance of
151 SmcR ligand binding in *Vibrio* signaling and response.
152
153

Results

A forward genetic screen identifies *smcR* alleles resistant to PTSP

Our previous study showed that substitutions F75Y or C170F rendered SmcR resistant to PTSP, whereas I96L and V140I did not affect PTSP sensitivity nor function (43). However, this was a limited reverse genetics experiment that encompassed only four substitutions in the putative LBP and did not determine if other residues are also involved in binding to ligand. To determine which SmcR residues are important for PTSP binding, we used a forward genetics approach in which we generated a *smcR* mutant library using random mutagenesis by error-prone PCR. The mutant libraries were assayed in a previously established dual-reporter bioassay in *E. coli* that contains *V. campbellii* promoters activated or repressed by LuxR/HapR-type proteins: 1) an activated reporter cassette comprising the *luxCDABE* promoter driving *gfp* expression, and 2) a repressed reporter cassette comprising the *05222* promoter driving *mCherry* expression (**Fig. 1B**) (19). Thus, in cells expressing wild-type *smcR*, GFP expression is high and mCherry expression is low. Conversely, in *smcR*-expressing cells in the presence of PTSP, GFP expression is low and mCherry expression is high, mimicking cells that do not express *smcR* (**Fig. 1C, 1D**). As with our previous reverse genetics assay, we sought to identify mutant *smcR* alleles that were resistant to PTSP and expressed GFP and mCherry at levels comparable to wild-type *smcR* cells in media without PTSP. Using flow cytometry, we sorted PTSP-treated cells based on their GFP and mCherry expression profiles into high and moderate resistance classes based on net difference in GFP values compared to DMSO-treated cells. (**Fig. 1C, 1D**). From screening ~60,000 mutant alleles, we identified multiple isolates with mutant *smcR* alleles with substitutions at residues F78, I96, M100, Q137, F166, H167, C170, and R179 (**Fig. 1C, 1D, Fig. S2**).

To assess the effect of substitutions in SmcR on QS regulation and growth, we focused on three PTSP-resistant *smcR* alleles with substitutions at H167, C170 and R179 and constructed isogenic mutant *V. vulnificus* strains. *V. vulnificus* utilizes various virulence factors, such as exotoxins and other biofilm-related factors for its persistence in the environment and pathogenesis during infection (43). We examined the effect of PTSP on protease activity. The *vvpE* gene encodes a protease, and this gene is known to be activated at HCD by SmcR activation (48). We hypothesized that the resistant mutant strains would exhibit no change in protease activity in the presence of PTSP but expected protease activity to decrease or be eliminated upon PTSP binding in the wild-type strain. First, we qualitatively measured each strain for growth and observed that the mutations did not lead to significant growth attenuation either in the presence or absence of PTSP (**Fig. S3**). We next measured protease activity in *V. vulnificus* supernatants using an azocasein-based assay. We observed that protease activity in wild-type *V. vulnificus* decreased ~10-fold upon treatment with 25 μm PTSP (**Fig. 1E**). Mutant strains treated with PTSP exhibited similar protease activities to the untreated cultures; although there were slight decreases in protease activity for each mutant, the only significant difference was in the strain expressing the SmcR variant R179C. We note that the protease activity of this mutant strain is significantly increased compared to wild-type in the untreated cultures, indicating that the R179C substitution somehow alters basal SmcR

activity, a point we return to below. From these data, we conclude that we have identified mutants of *smcR* that render SmcR resistant to PTSP and maintain and/or increase SmcR activity *in vivo*.

Previously, we had shown that PTSP binds *V. vulnificus* SmcR *in vitro* with greater affinity compared to *V. campbellii* LuxR (43). To determine if SmcR R179C could bind PTSP, we analyzed the binding affinity of PTSP to purified wild-type SmcR and the SmcR R179C variant by isothermal titration calorimetry (ITC). In its dimeric form, SmcR has two identical putative ligand-binding pockets. We incubated 10 μM of PTSP in the cell and titrated 100 μM of wild-type SmcR or SmcR R179C over 18 consecutive injections (**Fig. 1F, Fig. S4**). We found that the wild-type SmcR-PTSP interaction had a K_d of approximately 1 μM, while the SmcR R179C-PTSP interaction was sufficiently weak enough that a K_d could not be calculated (**Fig. 1G, Fig. S4**). These findings are consistent with the *in vivo* reporter data that showed that the SmcR R179C variant was recalcitrant to PTSP inhibition (**Fig. 1C**), further validating our structural and genetic approaches. These data suggest that PTSP binds SmcR specifically with ~1 μM affinity, and this interaction is disrupted in LBP variants of SmcR as observed with R179C.

PTSP binds to SmcR in the putative LBP

We used X-ray crystallography to determine the structural basis for the SmcR-PTSP interaction. We note that initial attempts to soak PTSP into already-formed SmcR protein crystals did not result in electron density maps that contained density consistent with a bound PTSP molecule, which was the method performed for the SmcR-Qstatin structure published (29). Instead, we added PTSP at the time of protein induction and screened for conditions that could promote crystallization of SmcR pre-bound to PTSP. We determined the structure of full-length SmcR bound to PTSP at 2.1 Å using molecular replacement (**Fig. 2A**; **Table S1; Movie S1**). The N-terminal DBD was largely disordered and residues 1-15 could not be modeled with high confidence and, thus, were not included in our final model (**Fig. S5A**). Additionally, the B-factors were high for residues in the more ordered region of the N-terminus (residues 16-62) that could be modeled compared to the rest of the structure (**Fig. S5A**). Indeed, it is possible this region of protein is actively unfolded or destabilized by the presence of PTSP, a point we address in our biochemical analyses of the SmcR-PTSP complex below. Conversely, the C-terminal domain, which contains the putative LBP, was well-ordered and allowed for the unambiguous placement of PTSP (**Fig. 2B, Fig. S5B**). The putative LBP is bipartite with distinct hydrophobic and hydrophilic regions, similar to what is observed in the ligand binding domains of LuxR-type proteins (49). One-half of the LBP is comprised of hydrophobic residues (F75, F78, L79, I96, M100, W114, F115, V140, F166, C170), which can accommodate the phenyl and pyrazole rings of PTSP (**Fig. 2B**). Additionally, the region of the LBP adjacent to the solvent accessible channel that allows for ligand accessibility to the binding site is lined with hydrophilic residues, which can act as a shield for the surrounding bulk solvent. Of note, residue R179 from one monomer of SmcR contacts water residues in the accessible ligand channel of the opposing monomer, potentially acting as a gate for ligand binding (**Fig. 2B; Fig. S5C)**. Furthermore, hydrophilic residues (N133, Q137, N164, H167) also contact water molecules and the thiophene head

228 group of PTSP (**Fig. 2B**). In particular, residue N133 forms an important hydrogen bond with the sulfonyl
229 group in PTSP (**Fig. 2B**). Nine of these residues were discovered as being important for binding to PTSP
230 in our forward genetic screen of SmcR or through reverse genetics (43) (**Fig. 1B, 1C, S5**), lending validity
231 to our model. Previous work in our lab revealed that HapR from *V. cholerae* was resistant to PTSP (41).
232 To understand the molecular basis for the selectivity of SmcR for PTSP, we compared the LBP of SmcR
233 to HapR. The most significant difference between the structures is at residues C170 in SmcR and F171 in
234 HapR (**Fig. S5D**). When the PTSP-bound structure of SmcR and the apo structure of HapR were
235 overlayed, residue F171 from HapR overlapped with the phenyl ring in PTSP, revealing a significant steric
236 clash that would prevent PTSP binding to HapR (**Fig. S5D**).
237 In recent years, SmcR and HapR have been targets for small molecule modulation for QS-
238 dependent repression of virulence (26–32, 41). SmcR and HapR variants bound to molecules possessing
239 similar moieties to PTSP have been solved, allowing us to determine the mechanism driving receptor
240 inactivation. In Fig. 2C, we overlayed the structures of SmcR-apo, SmcR-Qstatin, HapR (Y76F, L97I,
241 I141V and F171C)-IMT-VC-212 with a focus on the DBD of the receptors, specifically residue N55 in
242 SmcR (N56 in HapR), which we previously showed to be important for recognizing DNA to initiate
243 transcription (42). Typical of TetR receptors, SmcR and HapR both have an extended α-helix (residues
244 60-84) that connects the putative LBP and the DBD. In the SmcR-PTSP structure, the first α-helix of the
245 DBD is largely disordered, resulting in a displacement of N55, allowing the residue to point inward toward
246 the core of the DBD rather than the bulk solvent (**Fig. 2C**; **Fig. S5E**). Collectively, from these data, we
247 conclude that PTSP forms specific interactions with the LBP of SmcR, and alterations of the DBD
248 conformation, at the α-carbon backbone level, are observed in the PTSP-bound structure compared to
249 the apo-SmcR structure. However, due to the nature of the disordered N-terminus, we cannot reliably
250 determine the specific molecular interactions that might drive such a change.
251
252 **PTSP promotes SmcR flexibility in solution**
253 To assess the potential conformational changes induced by PTSP binding in solution,
254 we performed small-angle X-ray scattering (SAXS) experiments using SmcR-apo and SmcR-PTSP (**Fig.**
255 **S6 and S7**). Consistent with previous work (42), SAXS data collected for SmcR-apo fit well with high-
256 resolution X-ray structure data (PDB: 6WAE) (low χ^2, with a value of 0.80. We observed a poor fit of the
257 SmcR-PTSP SAXS data to high-resolution data, with a χ^2 value of 2.58 (**Fig. S8**, **Table S2**). This
258 observation agrees with our X-ray crystallographic data, in which we observed disordered regions in the
259 N-terminal DBD in the presence of PTSP. We hypothesized that these disordered regions are indicative
260 of partial protein unfolding. The SAXS data revealed that SmcR-apo adopted a radius of gyration (R_g) of
261 28.6 Å, whereas SmcR-PTSP adopted a R_g of 30.4 Å. R_g is defined as the root mean squared deviation of
262 the average of the distance of all electrons from the center of a particle as extrapolated from a Guinier
263 plot of the raw data at low angles. Thus, apo-SmcR adopts a more compact shape compared to SmcR-
264 PTSP, which has a more flexible structure in solution. Consistent with this, the pair-distance distribution

265 functions derived from the scattering profiles, which is a calculation of the distance between any two
266 atoms in a given volume, revealed an apo-SmcR profile with a bell-shaped curve and a single peak of a
267 P(r)/I(0) ratio of 0.00175 at a distance of ~35 Å, resembling a globular protein with a compact shape. In
268 contrast, the SmcR-PTSP scattering profile showed a smaller peak (P(r)/I(0) ratio of 0.00150) at a
269 distance of ~35 Å, with an elongated peak that extended to higher r values, suggesting a flexible region of
270 the protein and a potential conformational change in solution (**Fig. 2D, Table S2)**. Overall, these data
271 suggest that SmcR in the presence of PTSP undergoes partial unfolding in solution as compared to
272 SmcR-apo.
273
274 **PTSP increases proteolytic degradation of SmcR *in vivo***
275 From our structural and genetic experiments, we established that PTSP interacts with SmcR by
276 binding in its LBP. Our mutational analyses identified gain-of-function mutants of SmcR that were
277 resistant to PTSP activity *in vivo*. We hypothesized that this resistance phenotype was due to decreased
278 or eliminated PTSP binding. However, this phenotype could also be due to increased expression of SmcR
279 variant proteins compared to wild-type SmcR. Thus, we examined SmcR protein expression in strains
280 expressing wild-type and mutant *smcR* alleles in isogenic *V. vulnificus* mutant strains by western blot
281 analysis. In the wild-type strain, we observed a significant reduction of SmcR protein levels in the
282 presence of PTSP (**Fig. 3A, 3B, Fig. S9A-C**). Conversely, mutant strains expressing SmcR R179C,
283 SmcR H167Q, and SmcR C170F variants did not show altered expression levels of these proteins
284 comparing levels with or without PTSP added (**Fig. 3A, 3B, Fig. S9A-C**). However, the R179C mutant
285 showed overall increased expression compared to wild-type SmcR regardless of the presence or
286 absence of PTSP, correlating with its increased protease activity (**Fig. 3A, 4B, Fig. S9A-C**). We observed
287 similar results with *smcR* mutant alleles when measuring SmcR protein levels in the *E. coli* strains from
288 the genetic screen (**Fig. S9E**).
289 Next, we tested whether the decrease in SmcR levels upon PTSP addition was specific to this
290 compound or a general effect of thiophenesulfonamide inhibitors. We assayed a select number of
291 thiophenesulfonamide inhibitors that we previously synthesized and characterized *in vivo* (**Fig. 3C**). Each
292 of the compounds tested resulted in an average decrease in SmcR levels compared to the DMSO solvent
293 control (**Fig. 3D, 3E, Fig. S10A-C**). For all compounds, the decreased levels of SmcR correlated with the
294 inhibitor efficacy determined for *V. vulnificus in vivo*. For example, 10A and PTSP were the strongest
295 inhibitors with the lowest IC_{50}s against *V. vulnificus* (1 nM and 2 nM, respectively) (43) and also displayed
296 the largest average decreases in SmcR levels *in vivo*. Conversely, Qstatin and 3B had modest-weak
297 efficacy and higher IC_{50} values against *V. vulnificus* SmcR (0.5 μM and 0.9 μM), respectively, and the
298 addition of these Qstatin only moderately-poorly decreased SmcR levels (**Fig. 3D, 3E, Fig. S10A-C**). We
299 conclude that degradation of SmcR correlates with thiophenesulfonamide IC_{50}.
300 To determine the relative stability SmcR in the presence or absence of PTSP, we treated cells
301 with PTSP and monitored SmcR protein stability over time following translation inhibition via

302 chloramphenicol treatment. With this assay, we observed SmcR protein degradation in *V. vulnificus*
303 treated with PTSP as early as 30 minutes post addition of chloramphenicol and lower protein
304 concentrations throughout the time course, whereas cultures not treated with PTSP showed increasing
305 SmcR levels throughout the 3-hour time course (**Fig. 4A, 4B, Fig. S11A-C**).
306 In our previous publication, we demonstrated that thiophenesulfonamides inhibit the SmcR-type
307 proteins of multiple *Vibrio* species, including *V. campbellii*, *V. parahaemolyticus*, and *V. coralliilyticus*,
308 though to different extents due to the conservation of their LBPs (43). To test if the degradation of SmcR
309 by thiophenesulfonamides is the same mechanism in other species, we assayed degradation in *V.*
310 *campbellii* and *V. parahaemolyticus* following chloramphenicol treatment. We observed degradation of
311 LuxR (*V. campbellii*) and OpaR (*V. parahaemolyticus*) in cultures treated with PTSP compared to the
312 DMSO controls (**Fig. 4C-F, Fig. S12A-C, Fig. S13A-C**). Much like SmcR, no degradation of LuxR or
313 OpaR was observed in the DMSO-treated cultures, supporting previous observations that these proteins
314 are highly stable *in vivo* (19, 20). From these results, we conclude that treatment of cells with
315 thiophenesulfonamides results in degradation of SmcR/LuxR/OpaR protein levels *in vivo*. Further, we
316 conclude that substitutions of specific PTSP-interacting residues stabilize and/or increase SmcR protein
317 levels *in vivo*.
318
319 **PTSP binding stimulates the ClpAP protease to degrade SmcR**
320 SmcR and its homologue HapR have been shown to be degraded by the ClpAP protease *in vivo*
321 (50–52). Further, SmcR is degraded by Lon protease under increased heat stress in *V. vulnificus* clinical
322 isolate MO6-24/0 (50). Thus, we hypothesized that PTSP binding altered SmcR degradation by ClpAP
323 and/or Lon proteases. To test this, we obtained the same strains from these previous studies (a kind gift
324 from Kyung-Jo Lee and Kyu-Ho Lee) and assayed SmcR levels in wild-type, Δ*clpX*, Δ*clpA*, Δ*clpP*, and
325 Δ*lon* mutants of *V. vulnificus* clinical isolate MO6-24/0 in the presence of PTSP or DMSO via western blot.
326 First, we verified that the observations we had made in the *V. vulnificus* ATCC 27562 strain were
327 consistent in the MO6-24/0 strain; we observed SmcR was also degraded in the presence of PTSP (**Fig.**
328 **6A**). Next, we assayed the levels of SmcR in isogenic strains containing deletions in *ΔclpA*, *ΔclpX*, *ΔclpP*,
329 and *Δlon* strains. We observed that deletion of *clpA* and *clpP* but not *clpX* or *lon* increased SmcR levels
330 (**Fig. 5A, 5B, Fig. S14**). This result is similar to what was observed for HapR in *V. cholerae* (52). Next, we
331 examined SmcR levels in the PTSP treatment compared to the DMSO control, and again we observed
332 that wild-type SmcR decreased in the presence of PTSP, as well as in the Δ*clpX* and Δ*lon* strains.
333 However, in the Δ*clpA* and Δ*clpP* strains, SmcR levels were similar with or without PTSP treatment (**Fig.**
334 **5A, 5B, Fig. S14**). From these results, we conclude that that SmcR is a substrate for the ClpAP protease,
335 and binding of PTSP to SmcR makes it more susceptible to proteolytic cleavage by ClpAP.
336
337 **SmcR degradation controls the timing of the switch in phenotype between high- to low- cell**
338 **density**

339 The protein levels of SmcR in the cell are controlled by the QS pathway; HCD cultures produce
340 ~10-fold more SmcR protein than is produced at LCD (19, 53). Because the level of SmcR protein
341 controls the expression of downstream genes, we hypothesized that ClpAP-mediated degradation of
342 SmcR impacts the timing of the switch between densities. To test the effect of SmcR degradation – either
343 by ClpAP or by PTSP – we used bioluminescence expression to examine the QS-state of the cell. We
344 have previously shown that bioluminescence, produced by genes *luxCDABE* and activated by LuxR in *V.*
345 *campbellii*, is direct readout of SmcR-type protein levels in multiple *Vibrio* species (19, 43, 54, 55). We
346 constructed and tested mutant alleles in *V. vulnificus* that have defined QS phenotypes in other *Vibrio*
347 species. A *luxO D60E* mutant is a phosphomimic that constitutively activates the Qrr sRNAs and behaves
348 as a LCD-locked strain (*i.e.*, low expression of SmcR) (**Fig. S1**). Conversely, a Δ*luxO* strain does not
349 activate Qrrs and has constitutively high levels of SmcR, and thus it behaves as a HCD-locked strain (**Fig.**
350 **S1**). Using a plasmid with the native *luxCDABE* bioluminescence locus derived from *V. campbellii*, we
351 assessed the bioluminescence phenotypes of these mutant strains compared to wild-type. We observed
352 that wild-type *V. vulnificus* produced a standard "U-shaped" curve; as HCD overnight cultures are back-
353 diluted into fresh medium (autoinducers are diluted out), the bioluminescence decreases (**Fig. 6A, Fig.**
354 **S15, Fig. S16A**). Throughout the growth curve, autoinducers accumulate, and when the cell density
355 reaches quorum, the bioluminescence is activated and becomes maximal at HCD (**Fig. 6A, Fig. S15, Fig.**
356 **S16A**). Addition of PTSP to wild-type upon back-dilution into fresh medium resulted in complete loss of
357 bioluminescence over time (**Fig. 6A, Fig. S15, Fig. S16A**). The Δ*luxO* strain was constitutively bright in
358 the absence of PTSP, but the bioluminescence decreased to background levels when this strain was
359 treated with PTSP (**Fig. 6A, Fig. S16A**). Both the Δ*smcR* and *luxO D60E* strains were constitutively dark
360 in the presence or absence of PTSP. From these data, we conclude that addition of PTSP to wild-type or
361 Δ*luxO* cultures results in loss of bioluminescence, indicating that SmcR level and degradation by PTSP is
362 epistatic to the Δ*luxO* allele.
363 Using this bioluminescence assay, we sought to examine the impact of ClpAP degradation of
364 SmcR during the transitions between HCD to LCD, and also from LCD to HCD. We hypothesized that
365 deletion of either *clpA* or *clpP* would increase SmcR levels and thus bioluminescence expression
366 throughout the curve, delating the transition between HCD to LCD and increasing the transition between
367 LCD to HCD. First, comparing only the untreated strains (DMSO control), the Δ*clpP* mutant was delayed
368 in the HCD to LCD transition compared to wild-type and increased to a higher final bioluminescence level
369 (**Fig. 6B, Fig. S16B**). Conversely, the Δ*clpA* mutant had lower bioluminescence levels compared to wild-
370 type throughout the curve (**Fig. 6B, Fig. S16B**). All PTSP-treated strains decreased levels of
371 bioluminescence that reached basal levels at the end of the curve (**Fig. 6B, Fig. S16B**). Initially, we were
372 puzzled by the Δ*clpA* result; our hypothesis had been correct for Δ*clpP*, but not Δ*clpA*. However, upon
373 reading literature in the field, previous studies have shown that in *Caulobacter*, deletion of *clpA* increased
374 Lon levels (56). Thus, we hypothesize that in the absence of *clpA*, Lon targets SmcR for degradation
375 more than in wild-type. Further, we note that treatment of the Δ*clpP* mutant with PTSP still resulted in loss

376 of bioluminescence. This may also be due to increased levels of Lon activity. We note that the Δ*clpA* and
377 Δ*clpP* strains are in the MO6-24/0 *V. vulnificus* background, whereas the other strains in this experiment
378 were in ATCC 27562. To verify that the phenotypes we observed also occurred in the ATCC 27562 strain,
379 we constructed isogenic Δ*clpA* and Δ*clpP* mutants in that strain background and assayed
380 bioluminescence. The results were similar to the MO6-24/0 strain: in the absence of PTSP treatment, the
381 *ΔclpA* strain had slightly decreased bioluminescence compared to wild-type, whereas Δ*clpP* had
382 increased bioluminescence (**Fig. S17A-C**). After treatment with PTSP, both mutants had basal levels of
383 bioluminescence, indicating that the SmcR protein in these mutant strains is still susceptible to PTSP-
384 mediated degradation.
385 To further determine the role of SmcR degradation in HCD-LCD-HCD transitions, we assessed
386 the three mutant *smcR* alleles R179C, H167Q, and C170F, that increased SmcR stability to varying
387 degrees. We observed several distinctions in transition timing in untreated cultures (**Fig. 6C, Fig. S16C**).
388 First, each of the mutants exhibited a consistent delay in the switch from HCD to LCD compared to wild-
389 type, with the R179C mutant being the strongest phenotype. Second, each of the mutants exhibited
390 strong differences in the transition from LCD to HCD, both earlier in timing and more bioluminescence
391 production than wild-type, again with R179C being the strongest phenotype. Third, all three mutants also
392 exhibited higher overall levels of bioluminescence than the wild-type throughout the growth curve. These
393 data are consistent with our biochemical assays and western blot analyses (**Fig. 1, Fig. 2, Fig. 3A)**. Next,
394 we examined the effects of adding PTSP to the cultures at back-dilution into fresh medium. We observed
395 that there was a decrease in the final bioluminescence levels for *smcR* H167Q and *smcR* C170F
396 compared to untreated cultures, indicating that these two mutants were still somewhat sensitive to PTSP
397 treatment (**Fig. 6C, Fig. S16C**). However, the R179C mutant produced higher levels of bioluminescence
398 than wild-type at HCD even when treated with PTSP (**Fig. 6C, Fig. S16C**). Collectively, from these
399 results, we made three conclusions: 1) ClpAP turnover of SmcR affects both QS transition states, 2) when
400 cultures are treated with PTSP, in the absence of ClpAP, another mechanism of SmcR turnover occurs,
401 and 3) the SmcR variant R179C is resistant to protein degradation.
402
403 **Discussion**
404
405 *Vibrio* species have served as cornerstone models for studying numerous bacterial behaviors,
406 including biofilm formation, virulence factor secretion, host-pathogen interactions, bacteriophage-host
407 evolution, signaling, and more (57–65). QS was discovered in *Vibrio* species and much of the system
408 knowledge in the field was established through research on QS in *Vibrio cholerae, Vibrio fischeri,* and
409 *Vibrio campbellii* (in a strain previously classified as *V. harveyi*). The identification of the master
410 transcriptional regulators at the center of the QS circuit that we call LuxR/HapR proteins led to the
411 discovery of key gene families regulated by QS: biofilms, motility, competence, toxins, etc. The first
412 structural assessment of this *Vibrio*-specific protein family focused on HapR, followed by similar studies of

413 *V. vulnificus* SmcR and *V. alginolyticus* LuxR. The high amino acid identity of these proteins is even
414 surpassed by the nearly identical tertiary structures of these proteins, which unsurprisingly bind to nearly
415 identical DNA sequences *in vivo*. The literature is thorough in examinations of LuxR/HapR promoter DNA
416 binding, gene regulons, and protein-protein interactions that drive the global activity of these proteins (18,
417 66–68). However, one key attribute of these proteins had not been evaluated: the ligand binding potential.
418 As a subset of the massive TetR protein family, LuxR/HapR proteins have a LBP clearly defined by an
419 open channel lined with hydrophilic residues and a hydrophobic core (26). Indeed, in every X-ray crystal
420 structure of the "apo" protein, there is density observed in the LBP, even though these proteins are
421 purified from *E. coli* (25, 26, 43). Yet no phenotype has been determined for one of these proteins without
422 its native ligand. Rather, a few studies have shown that inhibitors can bind LuxR/HapR proteins,
423 decreasing their transcriptional regulation activity *in vivo*. Studies of thiophenesulfonamide inhibitors such
424 as PTSP and Qstatin have likewise shown that these molecules bind specifically to LuxR/HapR proteins
425 with varying affinities (25, 43). However, the mechanism of action was not known. Assays *in vitro* for DNA
426 binding yielded no significant differences in binding affinity, yet *in vivo* the addition of these compounds
427 clearly blocked LuxR/HapR activity.
428 Here, we identified the mechanism of thiophenesulfonamide inhibition of LuxR/HapR proteins via
429 ClpAP degradation. We propose a model for SmcR degradation by ClpAP and its impact on QS transition
430 states in **Figure 7**. Our data show that SmcR binds thiophenesulfonamides in its LBP, and addition of
431 these compounds *in vitro* alters SmcR protein folding dynamics. We determined that
432 thiophenesulfonamides such as PTSP drive SmcR proteolysis via the ClpAP protease, hence blocking its
433 activity *in vivo*. Thus, we have uncovered the reason that *in vitro* DNA binding assays were not altered by
434 addition of PTSP nor Qstatin but only *in vivo* activity was changed. Armed with this clear and measurable
435 proteolysis phenotype driven by inhibitor binding, we now aim to uncover the role of the native ligand in
436 LuxR/HapR function *in vivo*.
437 The next question we aim to focus on is: how does inhibitor binding to SmcR result in increased
438 proteolysis? We hypothesize that this is accomplished via conformational changes, as is often observed
439 with ligand binding for TetR proteins (69). Although we have successfully solved the structure of SmcR
440 bound to PTSP, the structure itself does not indicate large conformational changes that might explain how
441 SmcR is targeted for proteolysis when bound to PTSP. This may be due to the limited nature of X-ray
442 crystallography in that the structures are not determined in solution, and not all possible conformations
443 may form crystals. Based on our SAXS profiles and pair-distance distribution functions, SmcR bound to
444 PTSP in solution adopts a more elongated and flexible conformation. This may be a potential mechanism
445 for targeted proteolysis. We thus propose a model in which PTSP (or thiophenesulfonamides in general)
446 binds to the LBP of each monomer in the LuxR/HapR protein, resulting in a conformational change that
447 increases proteolysis of the dimer by the ClpAP protease (**Fig. 7**), possibly by exposing a ClpA-
448 dependent degron. We also aim to examine whether there is an adaptor protein such as ClpS required for
449 proteolysis by ClpAP. Notably, the *clpS* mutant did not exhibit a change in HapR protein levels in *V.*

450 *cholerae* (52), suggesting that ClpS is not required for ClpAP-mediated proteolysis in that system. We
451 also note that even in a Δ*clpP* strain, PTSP addition resulted in loss of bioluminescence, suggesting that
452 another protease may contribute to SmcR degradation. We hypothesize that the other protease activity is
453 from Lon. Several lines of evidence support this: 1) deletion of *clpA* in *Caulobacter* increases Lon protein
454 levels (56), 2) Lon has been shown to target SmcR during heat stress (46), and 3) degradation-resistant
455 alleles of *smcR* had increased bioluminescence even in the presence of PTSP, indicating that these
456 alleles are resistant to all protein degradation. Future genetic studies of the genes required for
457 LuxR/HapR protein degradation and biochemical studies of ligand binding will inform the mechanism of
458 thiophenesulfonamide-driven protein proteolysis.
459 Recent studies have shown that QS inhibitors are feasible alternatives to traditional antibiotics
460 with demonstrated efficacy in infection models (31, 32). As these inhibitors do not affect bacterial viability,
461 they are hypothesized to generate less selective pressure for evolving resistance (33, 34). These factors
462 make them attractive targets for *Vibrio* QS inhibition and possibly treatments for *Vibrio* diseases. For
463 example, Qstatin markedly decreased virulence of three *Vibrio* species against the brine shrimp *A.*
464 *franciscana* (29). Together, these results provide insights into the mechanism of action of an effective QS
465 inhibitor that may be useful in controlling *Vibrio* virulence in aquaculture.
466 Broadly, our discovery that ClpAP-mediated degradation impacts *V. vulnificus* QS phenotype
467 states has many implications that are relevant to cell survival and proliferation in native environments.
468 Our current model is that the levels of SmcR are controlled by ligand binding, whether the ligand is an
469 agonist or antagonist. The turnover of SmcR by ClpAP protease (and likely also another protease such as
470 Lon) mediates transitions between cell density states. We can envision different scenarios for both
471 transitions. When cells are at HCD and shifted to LCD, such as dispersal from a biofilm or host, QS signal
472 concentrations would quickly drop. However, the level of SmcR starting at its most concentrated would
473 not respond as quickly as the kinase/phosphorylation state of the receptors and regulators or the mRNA
474 turnover. Thus, the proteolytic turnover of SmcR would increase the rapidity with which cells could alter
475 gene expression to be in the LCD state. When cells transition from LCD to HCD, as cells colonize a host
476 and build a biofilm, the sensitivity of the transition from LCD to HCD is dictated by the accumulation of
477 SmcR protein. The ClpAP-proficient wild-type strain exhibited a longer time to reach "quorum", suggesting
478 that the turnover of SmcR controls the timing of LCD to HCD transition. Further exploration of the
479 mechanisms of ClpAP-mediated SmcR proteolysis and how this is impacted by putative native ligands will
480 be necessary to fully understand the impact of SmcR turnover on QS gene expression timing.
481
482 **Materials and Methods**

483 *Bacterial strains and media*
484 All strains and plasmids from this study are listed in Table S3 and Table S5. *Escherichia coli* strains
485 DH10B and S17-1λpir were used for cloning, and BL21(DE3) was used for the overexpression of SmcR
486 proteins. All *E. coli* strains and derivatives were grown at 37°C shaking at 275 rpm in Lysogeny Broth (LB)

487 medium with appropriate antibiotics. *V. vulnificus* and *V. campbellii* strains and derivatives were grown
488 shaking at 275 rpm at 30°C in LB Marine (LM) medium (LB with 2% NaCl final concentration) with
489 appropriate antibiotics. Antibiotics were used at the following concentrations: kanamycin 40 µg/ml or 100
490 µg/ml (*E. coli* or *Vibrio*, respectively), chloramphenicol (10 µg/ml), and tetracycline (10 µg/ml).
491
492 *Compound synthesis*
493 Qstatin, PTSP, and all other derivatives used in this study were either synthesized as described in
494 Newman *et. al*, 2021.
495
496 *Random mutagenesis and flow cytometry*
497 The *smcR* mutant alleles were created using GeneMorph II EZClone Domain Mutagenesis Kit
498 (Stratagene) as per the company protocol targeting the *smcR* gene encoded on plasmid pJN22, which
499 expresses *V. vulnificus smcR* under control of the IPTG-inducible P_{tac} promoter (43). Mutant libraries were
500 transformed into S17-1λpir competent cells, pooled, and stored at -80°C. DNA was extracted from the
501 library and then transformed into competent cells of *E. coli* strain DH10B containing the pJV064 reporter
502 plasmid, selected on LB plates with kanamycin and chloramphenicol, pooled, and stored at -80°C.
503 Overnight cultures of the pooled library were back-diluted 1:1,000 into fresh LB media with
504 chloramphenicol (10 µg/ml), kanamycin (40 µg/ml) and IPTG (50 µm), treated with either DMSO or PTSP
505 (25 µm) and grown shaking at 30°C overnight. Aliquots were prepared for flow cytometry by making 1:100
506 or 1:1,000 dilutions in PBS 30 mins prior to flow. Mutant strains resistant to PTSP were isolated by sorting
507 cells with high GFP and low mCherry fluorescence on a FACS Aria II. Following sorting, colonies were
508 inoculated individually into fresh medium, grown to stationary phase, and stored at -80°C.
509
510 *Dual-reporter* E. coli *bioassay*
511 Overnight *E. coli* cultures containing either pJN22 or empty vector control pMMB67EH-kanR and
512 the pJV064 reporter were diluted 1:1000 into LB with chloramphenicol (10 µg/ml) and kanamycin (40
513 µg/ml) and aliquoted into black-welled, clear-bottomed 96-well plates to a final volume of 150 µl. PTSP
514 was resuspended in DMSO at a stock concentration of 10 mM and added to *E. coli* cultures at a final
515 concentration of 25 µM unless otherwise stated. DMSO was added as a negative control at equal final
516 concentration. 50 µM IPTG was also added to the wells to activate expression of *smcR*. The 96-well
517 plates were covered in microporous sealing tape and grown for 16-18 hr shaking at 275 rpm at 30°C. The
518 OD_{600} and GFP and mCherry fluorescence were measured on a BioTek Cytation plate reader.
519
520 *Molecular methods*
521 All PCR reactions were performed using Phusion HF polymerase (New England Biolabs). All
522 oligonucleotides were purchased from Integrated DNA Technologies (IDT), and those used in this study

523 are listed (Table S5). All mutant strains (Table S3) were confirmed by DNA sequencing (Eurofins). Three
524 plasmids were constructed by Twist Biosciences.
525
526 *SmcR protein purification*
527 His-tagged wild-type and mutant SmcR proteins were expressed and purified as described previously
528 (70) using an Akta Pure L FPLC with His-Trap and gel-filtration columns. For induction of His-tagged wild-
529 type and mutant His-SmcR in presence of PTSP, induction media were supplemented with 50 μM of
530 PTSP dissolved in DMSO. No additional PTSP was added to buffers during purification. Proteins were
531 stored in gel filtration buffer (25 mM Tris, 300 mM NaCl, 1 mM DTT, 5 mM EDTA at pH 7.5) at 4°C.
532
533 *In vivo* protein turnover assay
534 *Vibrio* strains were streaked on LM plates with kanamycin (100 μg/ml), spectinomycin
535 (200 μg/ml), or trimethoprim (10 μg/ml) and incubated overnight at 30°C. Colonies were inoculated in 2 ml
536 LM with kanamycin (100 μg/ml), spectinomycin (200 μg/ml), or trimethoprim (10 μg/ml) and incubated at
537 37°C until an OD_{600} = ~1.0. Cultures were diluted in 25 ml of LM to an OD_{600}=0.05 and incubated at 30°C
538 with shaking (275 rpm) until ~OD_{600} = 0.5 to 0.8. Chloramphenicol (10 ug/ml) was added to the cultures
539 and cells were harvested at different time points thereafter (0, 30, 60, 120, and 180 minutes) by
540 centrifuging at 14,000 rpm for 2 minutes. Pellets were resuspended in lysis buffer (1 ml 1x Bugbuster, 50
541 μg/ml lysozyme,1μl Benzonase, 1X Protease Inhibitor) to 0.01 ODs/μl to stop the reactions. Processed
542 samples were analyzed by western blot as per previous protocol (17) using anti-LuxR antibodies, and
543 anti-RpoB antibodies were used as loading control.

544 *V. vulnificus strain construction*
545 Isogenic strains containing mutations in *smcR* were generated by mutating wild-type *V. vulnificus*
546 strain ATCC 27562. All isogenic mutant strains were generated using natural transformation via *tfoX*
547 induction and MuGENT (71, 72) via oligonucleotides listed in Table S4. First, derivative cas-vv006 was
548 constructed in which a trimethoprim-resistance (Tm^R) cassette was inserted downstream of *smcR* at the
549 native locus. The cas-vv006 strain was then used as a template to amplify *smcR*-Tm^R and generate
550 targeting DNA to introduce substitutions into *smcR* via natural transformation. These DNA products were
551 then introduced into wild-type *V. vulnificus* and selected for on LM plates with trimethoprim (10 μg/ml). All
552 isogenic mutant strains were confirmed by sequencing at the *smcR* locus.
553
554 *V. vulnificus growth curves*
555 *Vibrio* strains were inoculated in 5 ml LM or M9 medium (supplemented with casamino acids and
556 1% tryptone) overnight at 30°C shaking at 275 rpm with kanamycin (100 μg/ml), gentamicin (10 μg/ml),
557 spectinomycin (200 μg/ml), or trimethoprim (10 μg/ml) to select for reporter plasmids as needed.
558 Overnight cultures were back-diluted 1:100,000 in LM or M9 medium with antibiotics, treated with 25 μm
559 PTSP or an equal volume of DMSO and transferred into clear-bottomed 96-well plate. The plate was

560 covered and incubated in a BioTek Cytation plate reader overnight with shaking at 275 rpm at 37°C for 22
561 hr. OD_{600} was measured at 30 min intervals throughout the overnight incubation period.
562
563 *Protease assays*
564 *Vibrio* strains were inoculated in 5 ml LM with kanamycin (100 µg/ml), spectinomycin (200 µg/ml),
565 or trimethoprim (10 µg/ml) and incubated overnight at 30°C shaking at 275 rpm. Overnight cultures were
566 back diluted 1:1,000 in 10 ml LM with kanamycin (100 µg/ml), spectinomycin (200 µg/ml) or trimethoprim
567 (10 µg/ml) and the cell mixture was equally aliquoted into test and control sets, with 5 ml culture per set.
568 PTSP was added to test reactions at a concentration of 25 µM while DMSO was added as a negative
569 control at equal final concentrations into control reactions. These cultures were grown for 16-18 hrs
570 shaking at 275 rpm at 30°C. After incubation, OD_{600} was measured (1:10 dilution of overnights), and 1 ml
571 of overnight undiluted cultures were pelleted in 1.7 ml micro centrifuge tube at 13,000 rpm for 10 min at
572 room temperature. 100 µl supernatant was transferred to a new clear 1.7 ml microcentrifuge tube and
573 incubated with 400 µL of 1% azocasein (0.01 mg/ml dissolved in dH_2O) for 2 hrs 30 min at 37°C. The
574 reaction was stopped by addition of 600 µl 10% trichloroacetic acid, and the tubes were further incubated
575 on ice for 30 min, then centrifuged at 13,000 rpm for 5 min at room temperature. 800 µl of the protease
576 reaction was transferred to a new clear microcentrifuge tube, and 200 µl of 1.8 N NaOH was added.
577 OD_{420} was measured in a desktop spectrophotometer. Protease activity was calculated by dividing
578 OD_{420} by OD_{600}. Each assay was performed in technical and biological triplicates.
579
580 *Western blots*
581 *Vibrio* strains were inoculated in 5 ml LM with kanamycin (100 µg/ml), spectinomycin (200 µg/ml),
582 or trimethoprim (10 µg/ml) and incubated overnight at 30°C shaking at 275 rpm. Overnight cultures were
583 back diluted 1:1,000 in 10 ml LM with kanamycin (100 µg/ml), spectinomycin (200 µg/ml), or trimethoprim
584 (10 µg/ml) and the cell mixture was equally aliquoted into test and control sets, with 5 ml culture per set.
585 PTSP was added to test reactions at a concentration of 25 µM while DMSO was added as a negative
586 control at equal final concentrations into control reactions. These were incubated at 30°C shaking at
587 275 rpm. Cells were harvested after 16 hours growth overnight otherwise specified and resuspended in
588 lysis buffer (1 ml 1x Bugbuster, 50µg/ml lysozyme,1µl Benzonase and 1X protease inhibitor) to an OD_{600}
589 of 0.01/µl and incubated at room temperature for 10 minutes. SDS sample buffer was added to 10 µl
590 lysate with fresh β-mercaptoethanol (10%), and samples were boiled for 10 mins at 95°C. Western blot
591 analyses were performed as previously described (19), except that new anti-LuxR antibodies were
592 generated through Cocalico against purified LuxR protein. In addition, the western blots were probed with
593 anti-RpoB as a loading control as previously described (Neoclone) (73).
594
595 *Purification of SmcR:PTSP for crystallographic studies*

596 His-tagged wild-type SmcR-PTSP was expressed and purified via Ni-affinity chromatography as
597 previously described. Induction of expression was performed in induction media supplemented with 50
598 μM PTSP in DMSO. Clarified cell lysates were incubated with Ni-NTA running buffer equilibrated
599 NEBExpress Ni Resin for 1 hour with rocking at 4°C. Incubated resin was applied to a gravity column and
600 washed with 100 mL Ni-NTA running buffer. His-tagged wild-type SmcR-PTSP was eluted in 10 mL Ni-
601 NTA elution buffer in 1 mL fractions. Peak fractions, confirmed by SDS-PAGE, were pooled, and
602 concentrated to 1 mL over a 10 kDa MWCO filter (Amicon) for injection on a Superdex-200 size exclusion
603 column (Cytiva) equilibrated with gel-filtration buffer (25 mM Tris-HCl pH 7.5, 200 mM NaCl, 1 mM DTT).
604 Peak fractions, determined by 280 nm absorbance and confirmed by SDS-PAGE, were pooled and
605 concentrated to 5.2 mg/mL in gel-filtration buffer. SmcR:PTSP was stored at 4°C for immediate
606 crystallographic screening.
607
608 *Isothermal calorimetry analysis*
609 PTSP was re-suspended in 100% DMSO to a final concentration of 333 mM and serial diluted into a
610 solution containing decreasing amount of DMSO and increasing amount of gel filtration buffer (200 mM NaCl,
611 25 mM Tris pH 7.5) to a final concentration of 10 μM PTSP with 0.15% DMSO in the buffer. SmcR-wild-type
612 and SmcR-R179C proteins were purified as described. Purified proteins were then denatured through dialysis
613 at room temperature in a buffer containing 500 mM NaCl, 25 mM Tris pH 7.5, 1 mM DTT and 8 M Urea for 4 h,
614 then switched to buffer containing 500 mM NaCl, 25 mM Tris pH 7.5, and 1 mM DTT for 4 h to remove any
615 potential natively bound ligands. Aggregates were also removed. The re-natured proteins were then dialyzed
616 against ITC buffer (200 mM NaCl, 25 mM Tris pH 7.5 and 0.15% DMSO) overnight, concentrated to ~4.5-6
617 mg/mL. A MicroCal PEAQ-ITC (Malvern) was used to measure protein-ligand binding affinity at 25°C. 84μM to
618 120 μM proteins (4.4 mg/mL to 6 mg/mL, calculated as dimers) in the syringe were titrated into 10 μM PTSP in
619 the cell, with 500 rpm stirring speed and thermal power recorded every 10s. Data were fitted and analyzed
620 through the PEAQ-ITC Analysis software (Malvern).
621
622 *Crystallographic studies*
623 Previous crystallographic conditions for the determination of the SmcR-apo and SmcR-Qstatin
624 structures did not yield crystals for SmcR-PTSP. Purified SmcR-PTSP (5.2 mg/mL) in gel-filtration buffer was
625 screened using a variety of kit solutions (Nextal and Hampton) using a Gryphon Crystallization Robot (ART
626 Robbins Instruments) and incubated at RT for 4 days. Optimization screens were performed using the hanging
627 drop vapor diffusion method in 24-well crystallization trays. Initial SmcR-PTSP crystals were grown by mixing
628 1 μL protein solution with 1 μL well solution (2.0 M $MgSO_4$, 0.1 M MES pH 6.5) and sealed over a 1 mL well
629 solution. After incubation for 24 hours at RT, SmcR-PTSP crystals were harvested, transferred to a PCR tube
630 containing well solution, and vortexed. Fragmented crystals were used to streak-seed new drops of 1:1
631 protein:well solution to optimize crystal order and size. We thank Ted and Artemis Andrus-Paczkowski for the
632 generous donation of their shed whiskers. Seeded SmcR-PTSP crystals formed after 24 hours incubating at

633 RT, were batch harvested and soaked in cryoprotectant (20% v/v glycerol, 0.1 M MES pH 6.5, 1.6 M $MgSO_4$)
634 for 10 min. After the cryoprotecting step, single crystals were mounted on a MiTeGen loop and flash frozen and
635 stored under liquid nitrogen.
636
637 *Data collection and structure solution*
638 X-ray diffraction data were collected at Brookhaven National Laboratory National Synchrotron Light
639 Source-II on the NYX beamline. Diffraction images were processed in XDS and data reduction was
640 performed using CCP4-8.0.013 and Aimless (74). Automated and manual structure solutions were
641 generated via molecular replacement using *MrBUMP* and *SHELXE-MR*, respectively (75). Molecular
642 replacement in MrBUMP fit two copies of *V. vulnificus* SmcR-Qstatin (PDB: 5X3R, seq. identity 100%)
643 chain A with waters, sulfate ions, and Qstatin removed. Results from MrBUMP were used for molecular
644 replacement in SHELXE-MR. Alternating rounds of manual and automated refinement were performed
645 using Coot v0.9.8.8 and REFMAC5 (76). Structural validation was performed using Molprobity. Graphics
646 were created using Chimera (77).
647
648 *Small angle X-ray scattering*
649 SAXS data were collected at the Cornell High Energy Synchrotron Source (CHESS) 7A1
650 beamline over multiple runs. For all runs, a 250 µM x 250 µM X-ray beam with a wavelength of 1.094 Å at
651 7.1×10^{11} photons s^{-1} was used and centered on a quartz capillary sample cell with a path length of 1.5
652 mm. 10, 1-second images were collected using a dual Pilatus 100K-S detector system (Dectris, Baden,
653 Sweden), covering a range of $q \approx 0.0079$-0.45 $Å^{-1}$. The 1D SAXS profiles were grouped by sample and
654 averaged, followed by buffer subtraction (25 mM Tris-HCl pH 7.5, 200 mM NaCl, and 1 mM DTT) within
655 BioXTAS RAW (v2.2.1) (78). The radius of gyration (R_g) and forward scattering intensity $I(0)$ were
656 estimated by Guinier fit analysis, and the pair distance distribution function analysis was done in GNOM
657 (79) utilizing the ATSAS software suite (80)v3.2.1-1) implemented in BioXTAS RAW (Hopkins et al., 2017)
658 (v2.2.1). The molecular weights were estimated in a concentration independent manner from the Porod
659 volume, V_p (81). Single-state modelling was performed using the FoXS server
660 (https://modbase.compbio.ucsf.edu/foxs/)(82, 83).
661
662 *Bioluminescence curves*
663 Bioluminescence assays were performed in *V. vulnificus* ATCC 27562 and MO6-24/0 strains
664 containing IPTG-inducible pCS38 *luxCDABE* reporter plasmid (70). Overnight cultures of *V. vulnificus*
665 were diluted to 1:100000 in M9 minimal medium (supplemented with casamino acids and 1% tryptone)
666 with gentamycin (100 µg/ml) and treated with 25 uM PTSP or an equal volume of DMSO in 96-well clear
667 bottom black assay plates. The plates were incubated shaking at 30°C for 48 h in the BioTek Cytation 3
668 Plate Reader or BioTek Synergy H1 Plate Reader with bioluminescence and OD_{600} readings taken every
669 30 minutes.

670

671 **Data analysis**

672

673 All kinetic data were processed using GraphPad Prism software (GraphPad Software, Inc). For statistical
674 significance tests, data were analyzed using GraphPad Prism to perform tests to conform the normal
675 distribution of the data (Shapiro-Wilk test) with subsequent parametric tests for significance (ANOVA
676 and/or t-tests) as indicated in the figure legends.

677

678 **Data availability**

679

680 The X-ray structure data for SmcR-PTSP has been deposited (PDB: 8W39). All other data that support
681 the conclusions of this study are contained or described within the text or supporting information.

682

683 **Acknowledgments**

684

685 We thank Dr. Giovanni Gonzalez-Gutierrez and Juan Nysschen at Indiana University for technical
686 support, and Dr. Kyung-Jo Lee for sending us *V. vulnificus* MO6-24/0 Δ*clpA*, Δ*clpP*, Δ*clpX*, and Δ*lon*
687 mutant strains. We also thank Cristina Landeta and the Landeta lab for helping with western blot
688 protocols. We thank Dr. Peter Chien for helpful discussions about ClpAP and Lon. This research used
689 resources of the National Synchrotron Light Source II (NSLS-II), a U.S. Department of Energy (DOE)
690 Office of Science User Facility operated for the DOE Office of Science by Brookhaven National
691 Laboratory under Contract NO. DE-SC0012704. The authors thank Kevin Battaile, Director of the NYX
692 beamline at NSLS-II at Brookhaven National Laboratory, for technical assistance during data collection.
693 We would like to thank the members of van Kessel lab for their support and thoughtful discussions.
694 Cartoon diagrams in Figures S1 and 7 were created with bioRender.

695

696 **Funding and additional information**

697

698 The project was supported by NIH training grant T32GM132066 and NSF REU award DBI-175710 to
699 MWB, NIH grant R01GM14436101 to JEP, and NIH grant R35GM124698 to JVK. This work is based on
700 research conducted at the Center for High-Energy X-ray Sciences (CHEXS), which is supported by the
701 National Science Foundation (BIO, ENG and MPS Directorates) under award DMR-1829070, and the
702 Macromolecular Diffraction at CHESS (MacCHESS) facility, which is supported by award 1-P30-
703 GM124166-01A1 from the National Institute of General Medical Sciences, National Institutes of Health,
704 and by New York State's Empire State Development Corporation (NYSTAR).

705

706 **References**

1. M. K. Jones, J. D. Oliver, Vibrio vulnificus: Disease and pathogenesis. *Infect Immun* [Preprint] (2009).

2. F. Feldhusen, The role of seafood in bacterialfoodborne diseases. *Microbes Infect* **2**, 1651–1660 (2000).

3. W. G. Hlady, K. C. Klontz, The Epidemiology of Vibrio Infections in Florida, 1981-1993. *Journal of Infectious Diseases* **173**, 1176–1183 (1996).

4. I. Coly, A. Gassama Sow, M. Seydi, J. Martinez-Urtaza, *Vibrio cholerae* and *Vibrio parahaemolyticus* Detected in Seafood Products from Senegal. *Foodborne Pathog Dis* **10**, 1050–1058 (2013).

5. F. Le Roux, *et al.*, The emergence of Vibrio pathogens in Europe: Ecology, evolution and pathogenesis (Paris, 11-12 March 2015). *Front Microbiol* **6** (2015).

6. J. Martinez-Urtaza, *et al.*, Spread of Pacific Northwest Vibrio parahaemolyticus Strain . *New England Journal of Medicine* **369**, 1573–1574 (2013).

7. B. A. Froelich, D. A. Daines, In hot water: effects of climate change on Vibrio–human interactions. *Environ Microbiol* [Preprint] (2020).

8. A. Newton, M. Kendall, D. J. Vugia, O. L. Henao, B. E. Mahon, Increasing rates of vibriosis in the United States, 1996-2010: Review of surveillance data from 2 systems. *Clinical Infectious Diseases* [Preprint] (2012).

9. L. Vezzulli, *et al.*, Climate influence on Vibrio and associated human diseases during the past half-century in the coastal North Atlantic. *Proc Natl Acad Sci U S A* **113**, E5062–E5071 (2016).

10. A. S. Akanda, J. K. Griffiths, R. Colwell, S. Islam, A. S. Jutla, Warming Oceans, Phytoplankton, and River Discharge: Implications for Cholera Outbreaks. *Am J Trop Med Hyg* **85**, 303–308 (2011).

11. J. Mohan Raj, *et al.*, Presence & mobility of antimicrobial resistance in Gram-negative bacteria from environmental samples in coastal Karnataka, India. *Indian Journal of Medical Research* **149**, 290 (2019).

12. J. Verma, *et al.*, Genomic plasticity associated with antimicrobial resistance in *Vibrio cholerae*. *Proceedings of the National Academy of Sciences* **116**, 6226–6231 (2019).

13. C. Fuqua, S. C. Winans, E. P. Greenberg, CENSUS AND CONSENSUS IN BACTERIAL ECOSYSTEMS: The LuxR-LuxI Family of Quorum-Sensing Transcriptional Regulators. *Annu Rev Microbiol* **50**, 727–751 (1996).

14. W. C. Fuqua, S. C. Winans, E. Peter Greenberg2, “MINIREVIEW Quorum Sensing in Bacteria: the LuxR-LuxI Family of Cell Density-Responsive Transcriptional Regulatorst” (1994).

15. C. M. Waters, B. L. Bassler, QUORUM SENSING: Cell-to-Cell Communication in Bacteria. *Annu Rev Cell Dev Biol* **21**, 319–346 (2005).

16. K. C. Tu, B. L. Bassler, Multiple small RNAs act additively to integrate sensory information and control quorum sensing in *Vibrio harveyi*. *Genes Dev* **21**, 221–233 (2007).

17. A. S. Ball, R. R. Chaparian, J. C. Van Kessel, “Quorum Sensing Gene Regulation by LuxR/HapR Master Regulators in Vibrios” (2017).

747 18. S. T. Rutherford, J. C. Van Kessel, Y. Shao, B. L. Bassler, AphA and LuxR/HapR reciprocally
748 control quorum sensing in vibrios. *Genes Dev* **25**, 397–408 (2011).

749 19. J. C. van Kessel, L. E. Ulrich, I. B. Zhulin, B. L. Bassler, Analysis of activator and repressor
750 functions reveals the requirements for transcriptional control by LuxR, the master regulator of
751 quorum sensing in Vibrio harveyi. *mBio* **4** (2013).

752 20. J. C. Van Kessel, S. T. Rutherford, Y. Shao, A. F. Utria, B. L. Bassler, Individual and combined
753 roles of the master regulators apha and luxr in control of the Vibrio harveyi quorum-sensing
754 regulon. *J Bacteriol* **195**, 436–443 (2013).

755 21. B. M. Henares, Y. Xu, E. M. Boon, A nitric oxide-responsive quorum sensing circuit in Vibrio
756 harveyi regulates flagella production and biofilm formation. *Int J Mol Sci* **14**, 16473–16484 (2013).

757 22. B. M. Henares, K. E. Higgins, E. M. Boon, Discovery of a nitric oxide responsive quorum sensing
758 circuit in vibrio harveyi. *ACS Chem Biol* **7**, 1331–1336 (2012).

759 23. R. R. Chaparian, S. G. Olney, C. M. Hustmyer, D. A. Rowe-Magnus, J. C. van Kessel, Integration
760 host factor and LuxR synergistically bind DNA to coactivate quorum-sensing genes in Vibrio
761 harveyi. *Mol Microbiol* **101**, 823–840 (2016).

762 24. K. Barrasso, *et al.*, Dual-function quorum-sensing systems in bacterial pathogens and symbionts.
763 *PLoS Pathog* **16** (2020).

764 25. Y. Kim, *et al.*, Crystal structure of SmcR, a quorum-sensing master regulator of Vibrio vulnificus,
765 provides insight into its regulation of transcription. *Journal of Biological Chemistry* **285**, 14020–
766 14030 (2010).

767 26. R. S. De Silva, *et al.*, Crystal structure of the Vibrio cholerae quorum-sensing regulatory protein
768 HapR. *J Bacteriol* **189**, 5683–5691 (2007).

769 27. L. Cuthbertson, J. R. Nodwell, The TetR Family of Regulators. *Microbiology and Molecular Biology*
770 *Reviews* **77**, 440–475 (2013).

771 28. E. Swartzman, M. Silverman, E. A. Meighen, The luxR gene product of Vibrio harveyi is a
772 transcriptional activator of the lux promoter. *J Bacteriol* **174**, 7490–7493 (1992).

773 29. B. S. Kim, *et al.*, QStatin, a selective inhibitor of quorum sensing in Vibrio species. *mBio* **9** (2018).

774 30. S. M. Kim, *et al.*, LuxR Homologue SmcR Is Essential for Vibrio vulnificus Pathogenesis and
775 Biofilm Detachment, and Its Expression is Induced by Host Cells. *Infect Immun* **81**, 3721–3730
776 (2013).

777 31. Q. Jiang, *et al.*, Quorum Sensing: A Prospective Therapeutic Target for Bacterial Diseases.
778 *Biomed Res Int* [Preprint] (2019).

779 32. B. Rémy, *et al.*, Interference in bacterial quorum sensing: A biopharmaceutical perspective. *Front*
780 *Pharmacol* [Preprint] (2018).

781 33. M. Starkey, *et al.*, Identification of Anti-virulence Compounds That Disrupt Quorum-Sensing
782 Regulated Acute and Persistent Pathogenicity. *PLoS Pathog* **10** (2014).

783 34. A. Guendouze, *et al.*, Effect of quorum quenching lactonase in clinical isolates of pseudomonas
784 aeruginosa and comparison with quorum sensing inhibitors. *Front Microbiol* **8** (2017).

785 35. G. Brackman, *et al.*, Structure-activity relationship of cinnamaldehyde analogs as inhibitors of AI-2
786 based quorum sensing and their effect on virulence of Vibrio spp. *PLoS One* **6** (2011).

787 36. G. Brackman, *et al.*, Cinnamaldehyde and cinnamaldehyde derivatives reduce virulence in Vibrio
788 spp. by decreasing the DNA-binding activity of the quorum sensing response regulator LuxR. *BMC*
789 *Microbiol* **8** (2008).

790 37. T. Defoirdt, *et al.*, A quorum sensing-disrupting brominated thiophenone with a promising
791 therapeutic potential to treat luminescent vibriosis. *PLoS One* **7** (2012).

792 38. T. Defoirdt, *et al.*, The natural furanone (5Z)-4-bromo-5-(bromomethylene)-3-butyl-2(5H)-furanone
793 disrupts quorum sensing-regulated gene expression in Vibrio harveyi by decreasing the DNA-
794 binding activity of the transcriptional regulator protein luxR. *Environ Microbiol* **9**, 2486–2495
795 (2007).

796 39. S. Rajamanikandan, J. Jeyakanthan, P. Srinivasan, Discovery of potent inhibitors targeting Vibrio
797 harveyi LuxR through shape and e-pharmacophore based virtual screening and its biological
798 evaluation. *Microb Pathog* **103**, 40–56 (2017).

799 40. S. Rajamanikandan, J. Jeyakanthan, P. Srinivasan, Binding mode exploration of LuxR-
800 thiazolidinedione analogues, e-pharmacophore-based virtual screening in the designing of LuxR
801 inhibitors and its biological evaluation. *J Biomol Struct Dyn* **35**, 897–916 (2017).

802 41. S. M. Kim, *et al.*, Phenotypic Discovery of an Antivirulence Agent against Vibrio vulnificus via
803 Modulation of Quorum-Sensing Regulator SmcR. *ACS Infect Dis* **6**, 3076–3082 (2020).

804 42. J. D. Newman, *et al.*, The DNA binding domain of the Vibrio vulnificus SmcR transcription factor is
805 flexible and binds diverse DNA sequences. *Nucleic Acids Res* **49**, 5967–5984 (2021).

806 43. J. D. Newman, *et al.*, Amino acid divergence in the ligand-binding pocket of Vibrio LuxR/HapR
807 proteins determines the efficacy of thiophenesulfonamide inhibitors. *Mol Microbiol* **116**, 1173–1188
808 (2021).

809 44. H. Sen, *et al.*, Diversity in the ligand binding pocket of HapR attributes to its uniqueness towards
810 several inhibitors with respect to other homologues - A structural and molecular perspective. *Int J*
811 *Biol Macromol* **233**, 123495 (2023).

812 45. F. Striebel, W. Kress, E. Weber-Ban, Controlled destruction: AAA+ ATPases in protein
813 degradation from bacteria to eukaryotes. *Curr Opin Struct Biol* **19**, 209–217 (2009).

814 46. W. Kress, Ž. Maglica, E. Weber-Ban, Clp chaperone–proteases: structure and function. *Res*
815 *Microbiol* **160**, 618–628 (2009).

816 47. G. Choi, S. H. Choi, Complex regulatory networks of virulence factors in Vibrio vulnificus. *Trends*
817 *Microbiol* **30**, 1205–1216 (2022).

818 48. H. S. Jeong, M. H. Lee, K.-H. Lee, S.-J. Park, S. H. Choi, SmcR and Cyclic AMP Receptor Protein
819 Coactivate Vibrio vulnificus vvpE Encoding Elastase through the RpoS-dependent Promoter in a
820 Synergistic Manner. *Journal of Biological Chemistry* **278**, 45072–45081 (2003).

821 49. A. R. McCready, J. E. Paczkowski, B. R. Henke, B. L. Bassler, Structural determinants driving
822 homoserine lactone ligand selection in the Pseudomonas aeruginosa LasR quorum-sensing
823 receptor. *Proc Natl Acad Sci U S A* **116**, 245–254 (2019).

824 50. K. J. Lee, Y. C. Jung, S. J. Park, K. H. Lee, Role of heat shock proteases in quorum-sensing-
825 mediated regulation of biofilm formation by Vibrio species. *mBio* **9** (2018).

826 51. F. I. Andersson, *et al.*, Structure and function of a novel type of ATP-dependent Clp protease.
827 *Journal of Biological Chemistry* **284**, 13519–13532 (2009).

828 52. C. A. Klancher, J. D. Newman, A. S. Ball, J. C. Van Kessel, A. B. Dalia, “Species-Specific Quorum
829 Sensing Represses the Chitobiose Utilization Locus in Vibrio cholerae” (2020).

830 53. C. M. Waters, B. L. Bassler, The *Vibrio harveyi* quorum-sensing system uses shared regulatory
831 components to discriminate between multiple autoinducers. *Genes Dev* **20**, 2754–2767 (2006).

832 54. S. A. Jung, C. A. Chapman, W.-L. Ng, Quadruple Quorum-Sensing Inputs Control Vibrio cholerae
833 Virulence and Maintain System Robustness. *PLoS Pathog* **11**, e1004837 (2015).

834 55. L. Plener, *et al.*, The Phosphorylation Flow of the Vibrio harveyi Quorum-Sensing Cascade
835 Determines Levels of Phenotypic Heterogeneity in the Population. *J Bacteriol* **197**, 1747–1756
836 (2015).

837 56. B. B. Barros, S. A. Mahmoud, P. Chien, R. D. Zeinert, Degradation of Lon in Caulobacter
838 crescentus. *J Bacteriol* **203** (2020).

839 57. J. C. N. Fong, K. A. Syed, K. E. Klose, F. H. Yildiz, Role of Vibrio polysaccharide (vps) genes in
840 VPS production, biofilm formation and Vibrio cholerae pathogenesis. *Microbiology (N Y)* **156**,
841 2757–2769 (2010).

842 58. D. A. Higgins, *et al.*, The major Vibrio cholerae autoinducer and its role in virulence factor
843 production. *Nature* **450**, 883–886 (2007).

844 59. A. J. Silva, J. A. Benitez, Vibrio cholerae Biofilms and Cholera Pathogenesis. *PLoS Negl Trop Dis*
845 **10**, e0004330 (2016).

846 60. K. L. Visick, An intricate network of regulators controls biofilm formation and colonization by *Vibrio*
847 *fischeri*. *Mol Microbiol* **74**, 782–789 (2009).

848 61. C. Murciano, L.-I. Hor, C. Amaro, Host–pathogen interactions in *Vibrio vulnificus* : responses of
849 monocytes and vascular endothelial cells to live bacteria. *Future Microbiol* **10**, 471–487 (2015).

850 62. D. R. Zamora-Pantoja, E. I. Quiñones-Ramírez, F. J. Fernández, C. Vázquez-Salinas, Virulence
851 factors involved in the pathogenesis of Vibrio parahaemolyticus. *Reviews in Medical Microbiology*
852 **24**, 41–47 (2013).

853 63. P. Kalatzis, D. Castillo, P. Katharios, M. Middelboe, Bacteriophage Interactions with Marine
854 Pathogenic Vibrios: Implications for Phage Therapy. *Antibiotics* **7**, 15 (2018).

855 64. F. J. Pollock, *et al.*, Visualization of coral host–pathogen interactions using a stable GFP-labeled
856 Vibrio coralliilyticus strain. *Coral Reefs* **34**, 655–662 (2015).

857 65. Y. Wei, P. Ocampo, B. R. Levin, An experimental study of the population and evolutionary
858 dynamics of *Vibrio cholerae* O1 and the bacteriophage JSF4. *Proceedings of the Royal Society B:*
859 *Biological Sciences* **277**, 3247–3254 (2010).

860 66. A. S. Ball, J. C. van Kessel, The master quorum-sensing regulators LuxR/HapR directly interact
861 with the alpha subunit of RNA polymerase to drive transcription activation in *Vibrio harveyi* and
862 *Vibrio cholerae*. *Mol Microbiol* **111**, 1317–1334 (2019).

863 67. J. Zhang, *et al.*, Binding site profiles and N-terminal minor groove interactions of the master
864 quorum-sensing regulator LuxR enable flexible control of gene activation and repression. *Nucleic*
865 *Acids Res* **49**, 3274–3293 (2021).

866 68. R. R. Chaparian, A. S. Ball, J. C. van Kessel, Hierarchical Transcriptional Control of the LuxR
867 Quorum-Sensing Regulon of Vibrio harveyi. *J Bacteriol* **202** (2020).

868 69. J. L. Ramos, *et al.*, The TetR Family of Transcriptional Repressors. *Microbiology and Molecular*
869 *Biology Reviews* **69**, 326–356 (2005).

870 70. J. D. Newman, J. C. van Kessel, "Purification of the Vibrio Quorum-Sensing Transcription Factors
871 LuxR, HapR, and SmcR" in *Methods in Molecular Biology*, (Humana Press Inc., 2021), pp. 173–
872 182.

873 71. A. B. Dalia, "Natural Cotransformation and Multiplex Genome Editing by Natural Transformation
874 (MuGENT) of Vibrio cholerae" in (2018), pp. 53–64.

875 72. T. N. Dalia, *et al.*, Multiplex Genome Editing by Natural Transformation (MuGENT) for Synthetic
876 Biology in *Vibrio natriegens*. *ACS Synth Biol* **6**, 1650–1655 (2017).

877 73. A. S. Ball, J. C. van Kessel, The master quorum-sensing regulators LuxR/HapR directly interact
878 with the alpha subunit of RNA polymerase to drive transcription activation in Vibrio harveyi and
879 Vibrio cholerae. *Mol Microbiol* **111**, 1317–1334 (2019).

880 74. M. D. Winn, *et al.*, Overview of the *CCP* 4 suite and current developments. *Acta Crystallogr D Biol*
881 *Crystallogr* **67**, 235–242 (2011).

882 75. R. M. Keegan, M. D. Winn, *MrBUMP* : an automated pipeline for molecular replacement. *Acta*
883 *Crystallogr D Biol Crystallogr* **64**, 119–124 (2008).

884 76. P. Emsley, K. Cowtan, *Coot* : model-building tools for molecular graphics. *Acta Crystallogr D Biol*
885 *Crystallogr* **60**, 2126–2132 (2004).

886 77. E. F. Pettersen, *et al.*, UCSF Chimera—A visualization system for exploratory research and
887 analysis. *J Comput Chem* **25**, 1605–1612 (2004).

888 78. J. B. Hopkins, R. E. Gillilan, S. Skou, *BioXTAS RAW* : improvements to a free open-source
889 program for small-angle X-ray scattering data reduction and analysis. *J Appl Crystallogr* **50**, 1545–
890 1553 (2017).

891 79. D. I. Svergun, Determination of the regularization parameter in indirect-transform methods using
892 perceptual criteria. *J Appl Crystallogr* **25**, 495–503 (1992).

893 80. D. Franke, *et al.*, *ATSAS 2.8* : a comprehensive data analysis suite for small-angle scattering from
894 macromolecular solutions. *J Appl Crystallogr* **50**, 1212–1225 (2017).

895 81. V. Piiadov, E. Ares de Araújo, M. Oliveira Neto, A. F. Craievich, I. Polikarpov, SAXSMoW 2.0:
896 Online calculator of the molecular weight of proteins in dilute solution from experimental SAXS
897 data measured on a relative scale. *Protein Science* **28**, 454–463 (2019).

898 82. D. Schneidman-Duhovny, M. Hammel, J. A. Tainer, A. Sali, Accurate SAXS Profile Computation
899 and its Assessment by Contrast Variation Experiments. *Biophys J* **105**, 962–974 (2013).

900 83. D. Schneidman-Duhovny, M. Hammel, J. A. Tainer, A. Sali, FoXS, FoXSDock and MultiFoXS:
901 Single-state and multi-state structural modeling of proteins and their complexes based on SAXS
902 profiles. *Nucleic Acids Res* **44**, W424–W429 (2016).

903

Figure 1

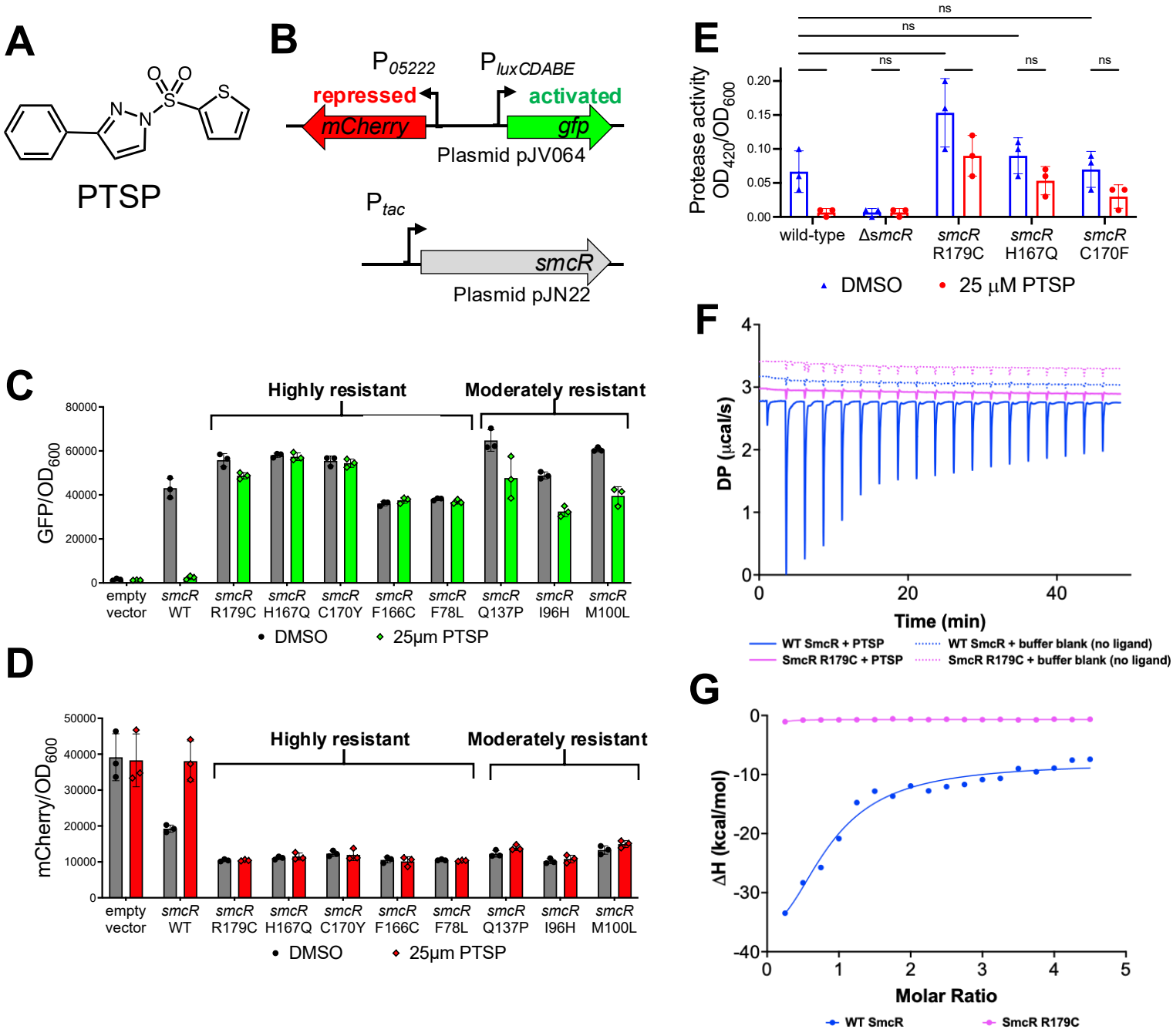

Figure 1. Forward genetic screen identifies mutant *smcR* alleles resistant to PTSP. (A) Structure of PTSP compound. (B) Diagram of the two-plasmid screen in *E. coli* in which wild-type or mutant *smcR* alleles encoded on plasmid pJN22 were screened for activity using a two-color reporter plasmid pJV064. The *luxCDABE* promoter is activated by SmcR and the *05222* promoter is repressed by SmcR. (C, D) *E. coli* strains contained plasmids pJN22 (wild-type *smcR* allele) or mutant pJN22 plasmids from library screening and pJV064. SmcR expression was induced with 50 μM IPTG and cultures treated with either 25 μM PTSP or an equal volume of DMSO solvent. GFP (C) and mCherry (D) relative to the OD_{600} were measured and plotted. (E) Protease activity (OD_{420}/OD_{600}) of wild-type and mutant *V. vulnificus* strains. (F) Representative isothermal titration calorimetry of WT SmcR (blue) and SmcR R179C (magenta) with (solid lines) or without (dotted lines) PTSP. (G) Transformed data from (F). DP and ΔH denote differential power and enthalpy, respectively. Statistical analyses: a two-way analysis of variance (ANOVA) was performed on normally distributed data (Shapiro-Wilk test; n=3; **, p=0.01; ***, p=0.001).

Figure 2

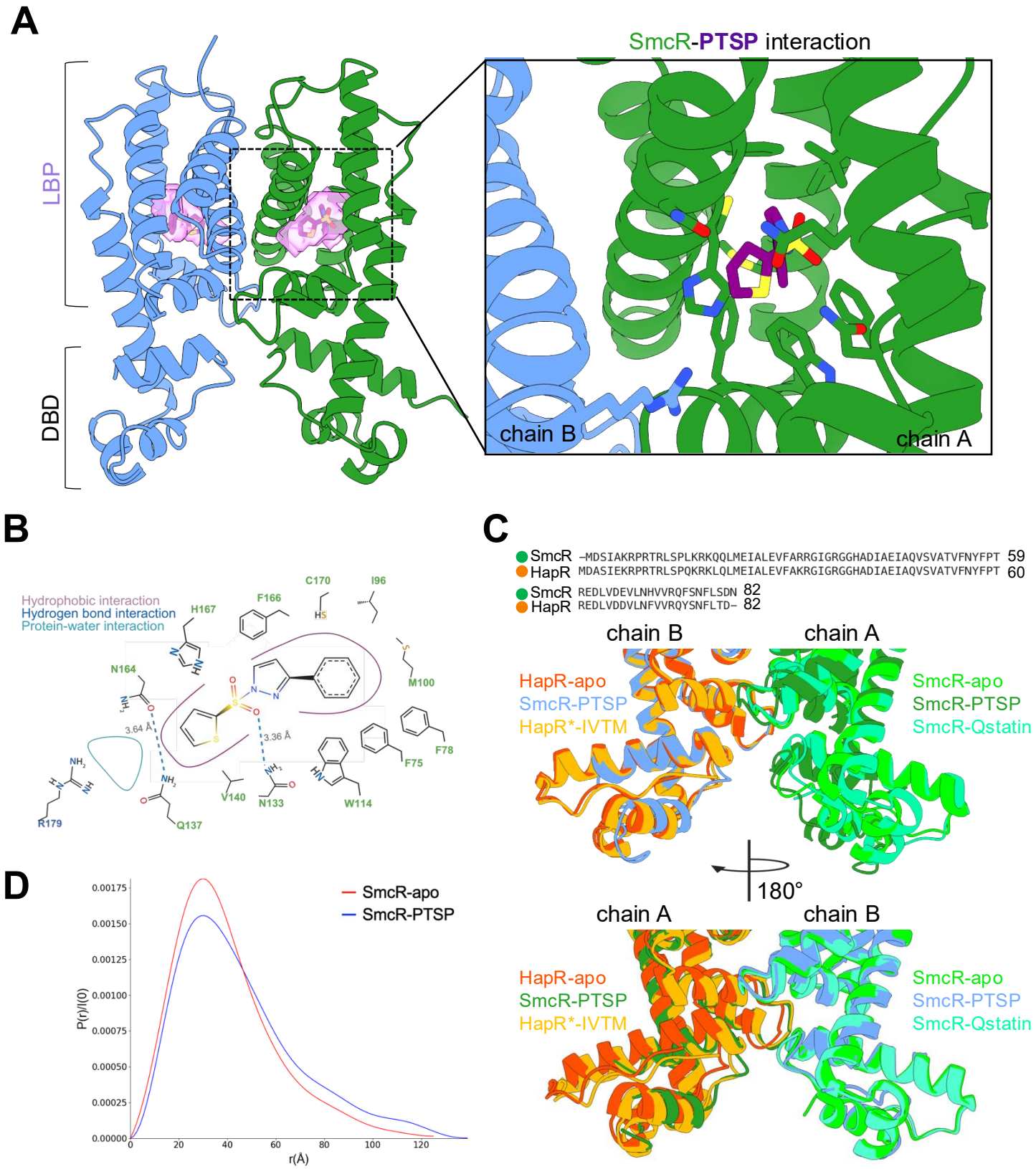

Figure 2. Structural basis for SmcR ligand binding. (A) X-ray crystal structure of homodimeric SmcR (blue/green) bound to PTSP (purple). Solvent accessible ligand binding pocket is shown as a surface in light purple (left). Residues important for contacting PTSP in the SmcR LBP (right). (B) 2D projection of the SmcR-PTSP binding interface showing hydrophobic contacts (purple lines), hydrogen bond interactions (blue), and solvent interactions (cyan). (C) Sequence and structural alignment of HapR and SmcR. The X-ray crystals structures of SmcR-apo (light green; PDB: 6WAE), SmcR-PTSP (colored by chain as in (A)) , SmcR-Qstatin (blue-green; PDB: 5X3R), HapR-apo (orange; 7XXO), and HapR*-ITVM (light orange; PDB: 7XYI). HapR* indicates the HapR quadruple variant from Sen et al. 2023 that stably binds to thiophenesulfonamide inhibitors. (D) The estimated pair-distance distribution function, P(r) normalized by the scattering intensity, I(0). The P(r) function is based on the Indirect Fourier Transform of SAXS data for SmcR-apo (red) and SmcR-PTSP (blue).

Figure 3

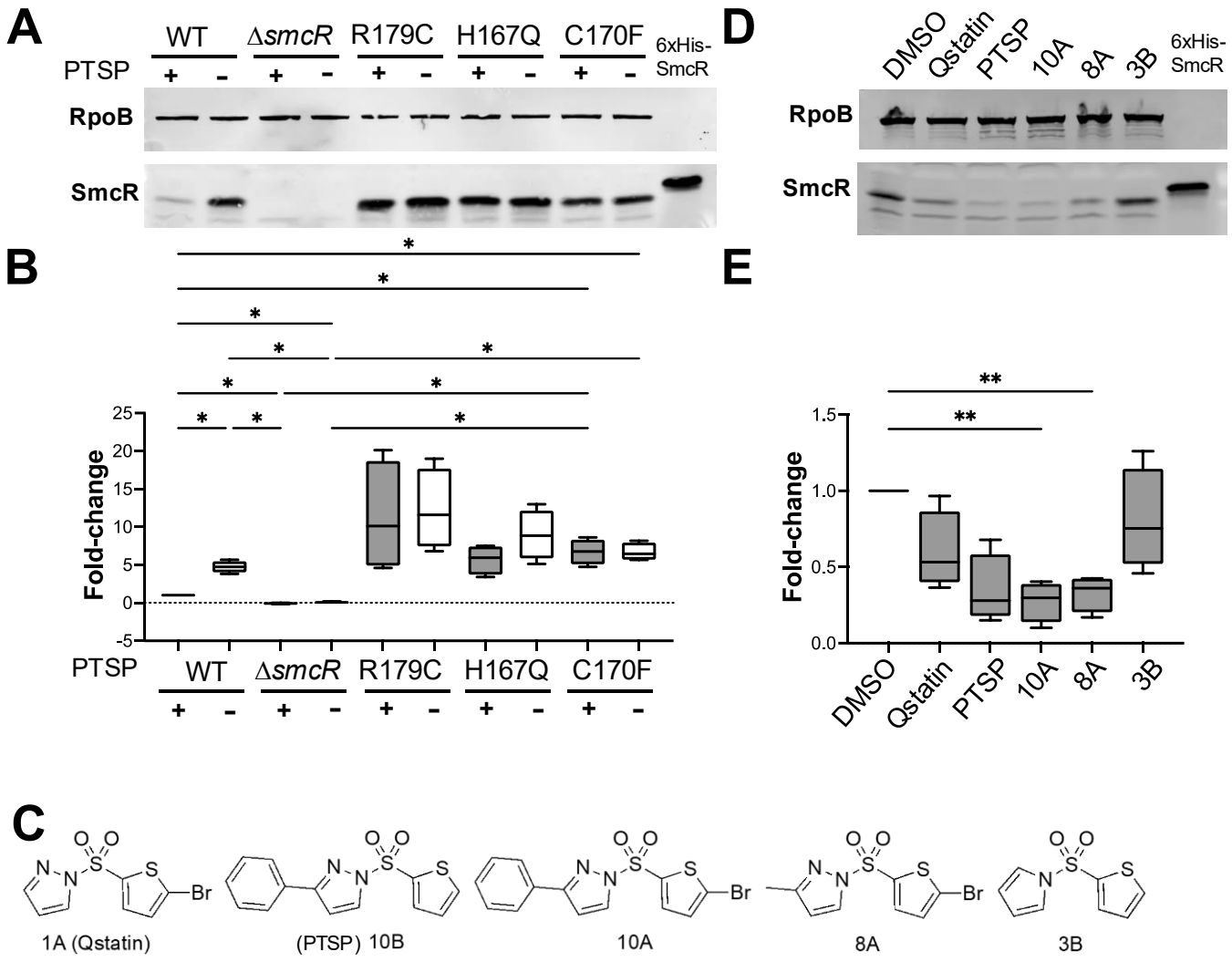

Figure 3. SmcR protein is degraded in the presence of PTSP. (A) Western blot analysis (representative of four biological replicates) of SmcR protein levels in cell lysates from *V. vulnificus* strains wild-type (WT), Δ*smcR* *smcR* R179C, *smcR* H167Q and *smcR* C170F. Strains were treated with 25 μM PTSP (+) or an equivalent volume of DMSO solvent (-). Anti-RpoB antibodies were used as a loading control. (B) Western blots of four biological replicates (shown in Fig. S9) were quantified with the SmcR band normalized to the RpoB band. Normally distributed data (Shapiro-Wilk test) were analyzed by one-way analysis of variance (ANOVA); *, $p < 0.05$, n=4. (C) Structures of thiophenesulfonamides used in panels A, B, D, and E. (D) Western blot analysis (representative of four biological replicates) of SmcR protein levels in cell lysates from WT *V. vulnificus* treated with 25 μM of each thiophenesulfonamide or an equivalent volume of DMSO solvent. Anti-RpoB antibodies were used as a loading control. (E) Western blots of four biological replicates (shown in Fig. S10) were quantified with the SmcR band normalized to the RpoB band. Normally distributed data (Shapiro-Wilk test) were analyzed by ANOVA; **, $p < 0.01$, n=4.

Figure 4

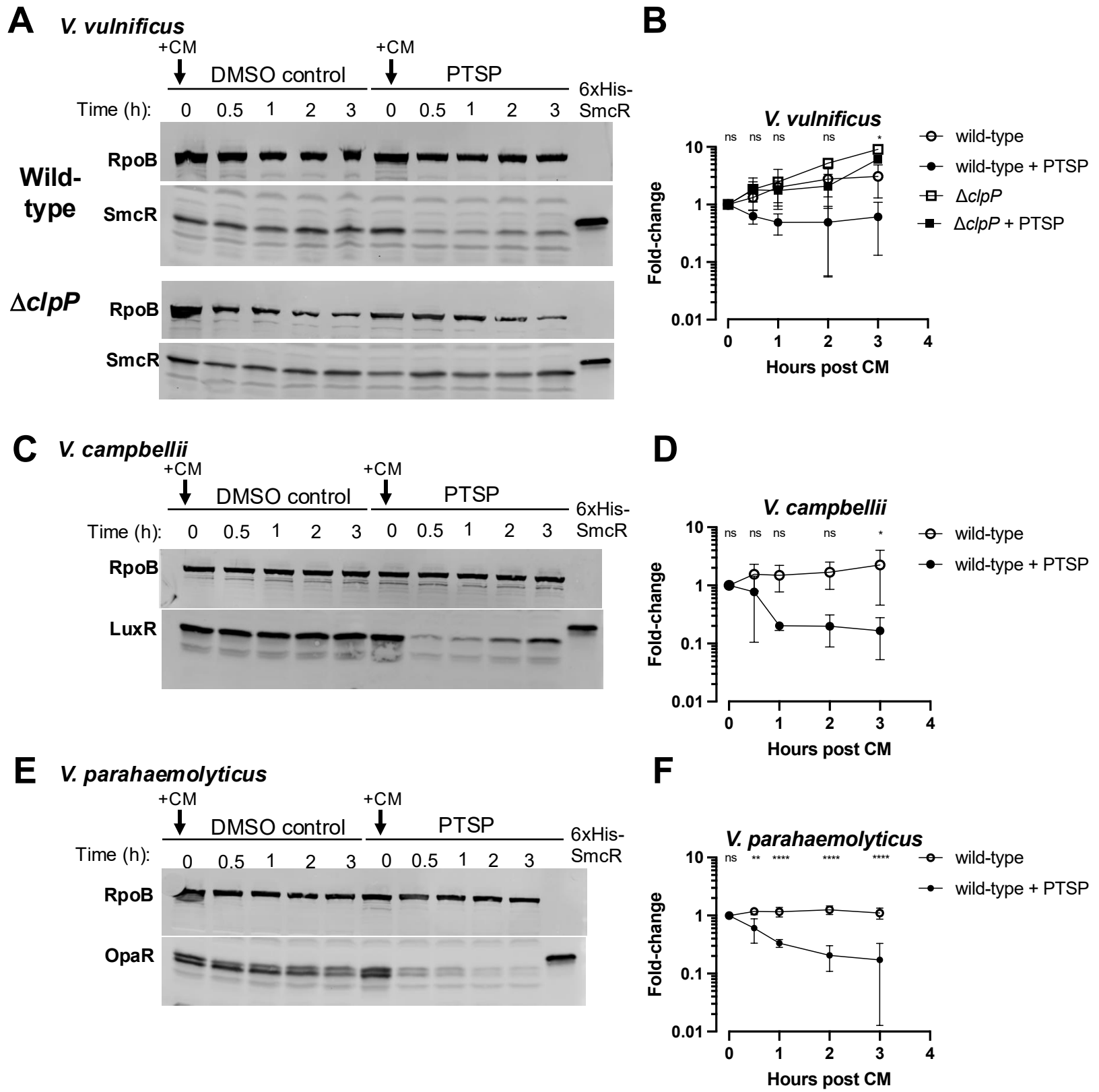

Figure 4. Time-course of SmcR proteins following translation inhibition. (A, C, E) Western blot analysis of cell lysates with anti-LuxR antibodies measuring SmcR from *V. vulnificus* (A), LuxR from *V. campbellii* (C), or OpaR from *V. parahaemolyticus* (E) (all wild-type strains). Cells were either treated with 25 μM PTSP or an equivalent concentration of DMSO solvent and grown to mid-log phase (OD_{600} = 0.5-0.8). Translation was halted by addition of 10 μg/ml of chloramphenicol (CM) at time 0, and pellets were harvested at 0, 30, 60, 120, and 180 mins. Anti-RpoB antibodies were used as a loading control. Each panel is a representative of triplicate biological assays (shown in Fig. S11, S12, S13). (B, D, F) Quantification of SmcR/LuxR/OpaR protein from triplicate biological replicates relative to the RpoB loading control are shown for each *Vibrio* species. Normally distributed data (Shapiro-Wilk test) were analyzed by ANOVA; *p<0.05,**, p<0.01, ****, p<0.0001; n=3. For panel B, the significant comparison is between wild-type and wild-type + PTSP.

Figure 5

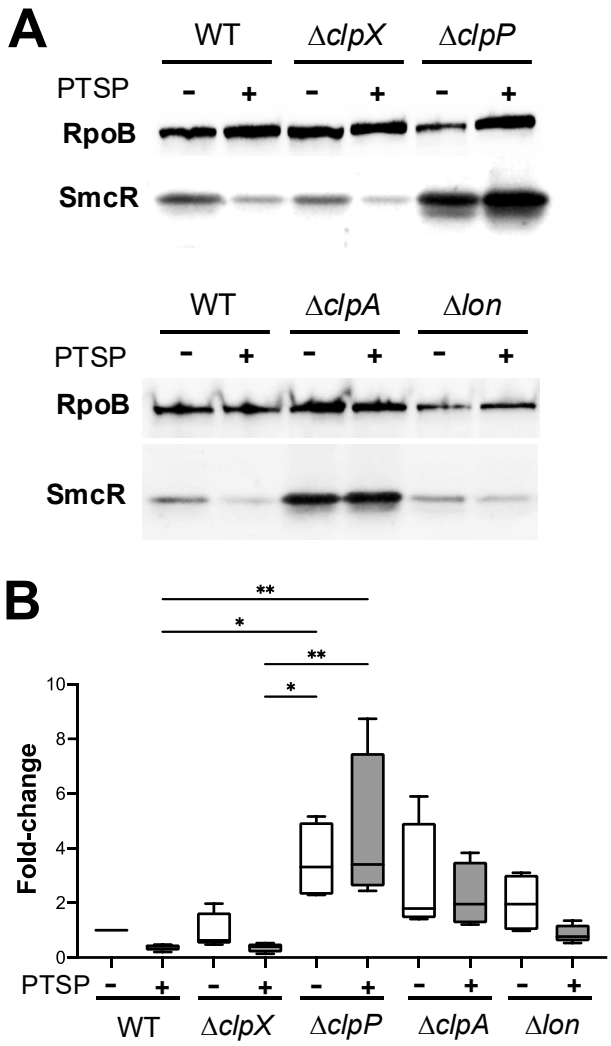

Figure 5. SmcR is proteolyzed by ClpAP. Western blot analysis of cell lysates measuring SmcR from *V. vulnificus* strain MO6-24/0 wild-type (WT), Δ*clpX*, Δ*clpP*, Δ*clpA*, and Δ*lon.* Strains were treated with 25 μM PTSP (+) or an equivalent volume of DMSO solvent (-). Anti-RpoB antibodies were used as a loading control. (B) Western blots of four biological replicates (shown in Fig. S14) were quantified with the SmcR band normalized to the RpoB band. Normally distributed data (Shapiro-Wilk test) were analyzed by ANOVA; *$p<0.05$,**, $p<0.01$, $n=4$.

Figure 6

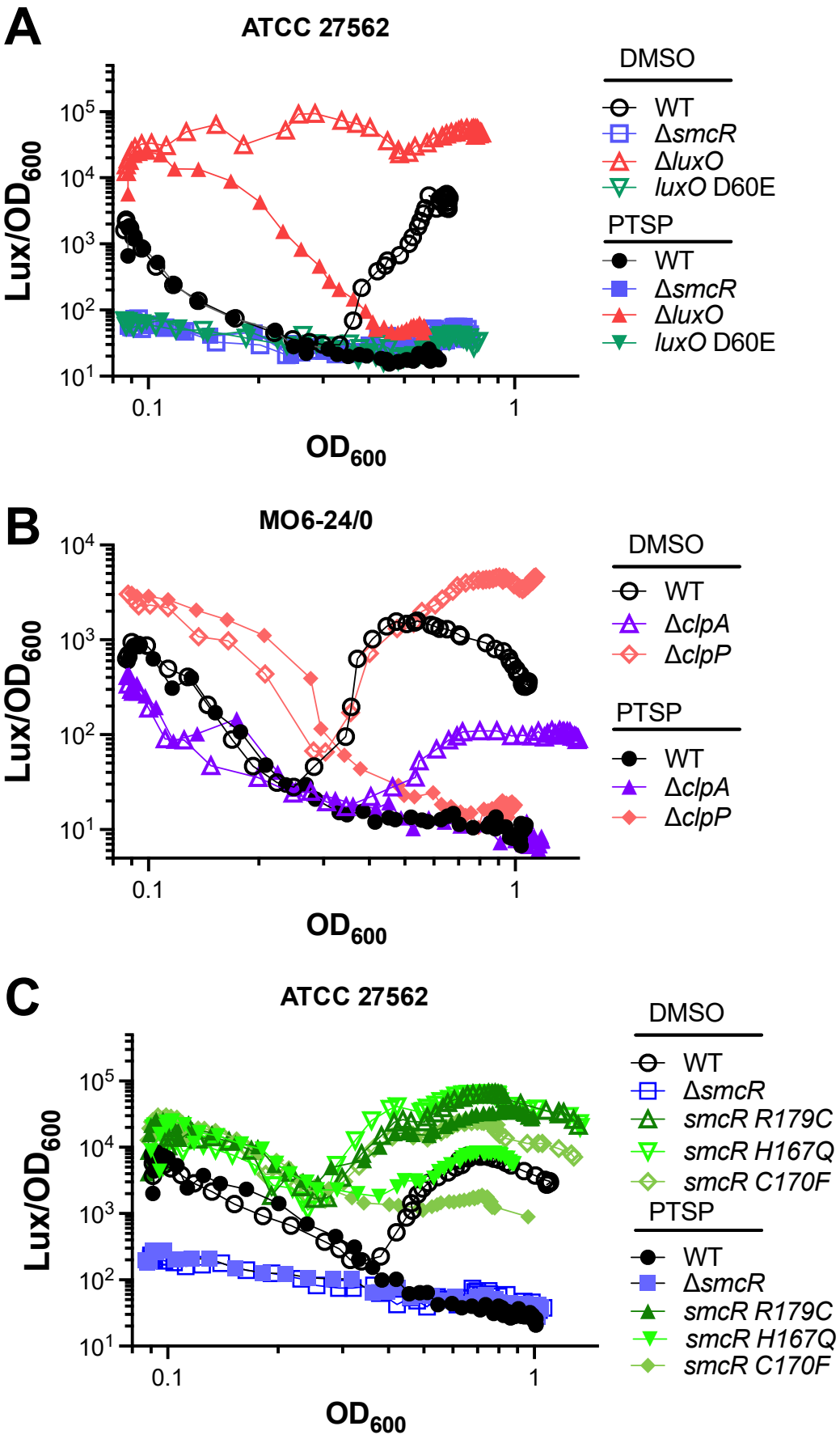

Figure 6. SmcR degradation controls the HCD to LCD transition. (A, B, C) Bioluminescence assays are plotted (Lux/OD_{600}) for *V. vulnificus* strains ATCC 27562 (A, C) and MO6-24/0 (B) wild-type (WT) and isogenic mutants. Strains were treated with 25 μM PTSP (+) or an equivalent volume of DMSO solvent (-) Figures are representative of triplicate biological assays (shown in Fig. S15).

Figure 7

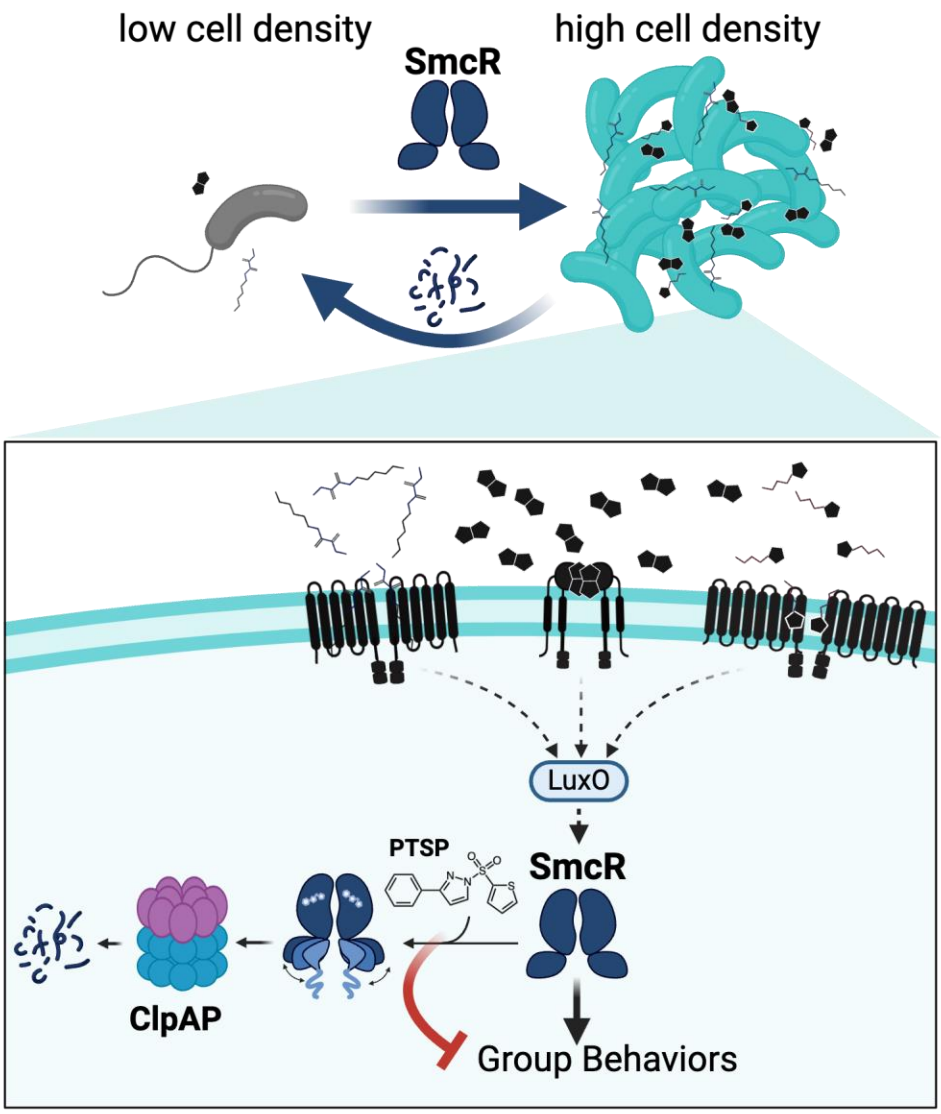

Figure 7. Model of the role of SmcR degradation in quorum sensing transitions. At low cell densities, low levels of autoinducers result in low levels of SmcR. As cells transition to high cell density, more SmcR is produced, which drives expression of group behavior genes. Our model is that SmcR is bound to its native ligand (unknown) and is most active at high cell density. As cells transition back to low cell density, degradation of SmcR by ClpAP increases the speed of this transition. Addition of inhibitor thiophenesulfonamide PTSP to cultures displaces the native ligand, driving an allosteric conformational change in the DNA binding domains of each SmcR monomer. We propose that the unfolded N-terminus is recognized by ClpAP and degraded, which blocks expression of group behavior genes. Image created with bioRender.